ELSEVIER

International Journal of Pressure Vessels and Piping 75 (1998) 375–396

INTERNATIONAL JOURNAL OF
Pressure Vessels and Piping

Crack-opening-area analyses for circumferential through-wall cracks in pipes—Part II: model validations

S. Rahman[a,*], F.W. Brust[b], N. Ghadiali[b], G.M. Wilkowski[b]

[a]*Department of Mechanical Engineering, The University of Iowa, Iowa City, IA 52242, USA*
[b]*Engineering Mechanics Group, Battelle, 505 King Avenue, Columbus, OH 43201, USA*

Received 31 May 1996; accepted 30 June 1997

Abstract

This is the second paper in a series of three papers generated from a recent study on crack-opening-area analysis of circumferentially cracked pipes for leak-before-break applications. This paper (Part II—Model Validations) focuses on the evaluation of current analytical models, discussed in the first paper (Part I—Analytical Models) as well as finite element models for conducting crack-opening-area analyses of pipes with circumferential through-wall cracks. The evaluation was performed by direct comparisons of the predicted results with the test data from full-scale pipe fracture experiments. The results from 25 full-scale pipe fracture experiments, conducted in the Degraded Piping Program, the International Piping Integrity Research Group Program and the Short Cracks in Piping and Piping Welds Program, were used to verify the analytical models. The main objective was the evaluation of engineering analysis procedures (estimation methods) as well as the ability of the finite element method to predict crack-opening displacements and shapes in pipes with circumferential through-wall cracks. Statistics were developed to quantify the accuracy of the current predictive models. A wide variety of pipe fracture tests involving cracks in base metals, weld metals and bimetallic weld metals were analyzed. Pipes containing both simple through-wall cracks and complex cracks were evaluated.

1. Introduction

The application of the leak-before-break (LBB) methodology requires the determination of leak rates. In addition to LBB analyses, which assume a hypothetical flaw size, there is also interest in the integrity of actual leaking cracks corresponding to current leakage detection requirements in the NRC Regulatory Guide 1.45 for assessing LBB applications where some cracking may be possible, or for assessing temporary repair of Class 2 and 3 pipes that have leaks as are being evaluated in ASME Section XI. For accurate leak-rate calculations, analytical models are needed to predict crack-opening area (COA) for a cracked pipe. For the prediction of crack-opening in a through-wall-cracked (TWC) pipe, it is desirable to have a mathematical model which is sufficiently accurate, relatively simple and inexpensive to use. For example, a detailed finite element analysis, while generally accurate, would have very limited use because it would be expensive and time-consuming to be used routinely. What is needed is a relatively simple equation, or a set of equations, to estimate the COA.

Besides the finite element method, there are a number of engineering (or estimation) methods available in the current literature to determine the crack-opening characteristics of a pipe with a circumferential crack. However, due to the lack of systematic studies involving combined experimental and analytical efforts, the accuracy of these methods for different pipe materials, crack geometries and loading conditions have yet to be evaluated.

In Rahman et al. [1] (Part I—Analytical Models), a comprehensive review was conducted to determine the current state-of-the art in predicting crack-opening displacement (COD) and fracture response for circumferentially cracked pipes under pure bending, pure tension and combined bending and tension loads. Based on that review, the following methods were identified for a systematic evaluation of their accuracy:

1. the GE/EPRI method [2–4];
2. the Paris/Tada method [5];
3. the LBB.NRC method; [6]
4. the LBB.ENG2 method [7–9];
5. the LBB.ENG3 method [10–12].

The details for each of these methods are given in Rahman et al. [1] and will not be repeated in this paper.

* Corresponding author.

0308-0161/98/$ - see front matter
PII: S0308-0161(97)00082-3

This paper (Part II—Model validations) focuses on the evaluation of the above analytical models as well as the finite element models for conducting crack-opening-area analyses of pipes with circumferential through-wall cracks. The evaluation was performed by direct comparisons of the predicted results with the test data from full-scale pipe fracture experiments. The results from 25 full-scale pipe fracture experiments, conducted in the Degraded Piping Program [13], the International Piping Integrity Research Group Programs (IPIRG) [14,15] and the Short Cracks in Piping and Piping Welds Program [16] were used to verify the analytical models. The main focus was on evaluating engineering analysis procedures (estimation methods) as well as the ability of the finite element method (FEM) to predict crack-opening displacements and shapes in pipes with circumferential through-wall cracks. A wide variety of pipe fracture tests involving cracks in base metal, weld metal and bimetallic weld metal were analyzed. Pipes containing both simple through-wall-cracks and complex-cracks were evaluated. The effects of off-center cracks, restraint of pressure-induced bending, thickness transition and weld residual stresses are discussed in a companion paper from this study [17].

2. Elastic–plastic finite element analyses

2.1. Past results

In the past, Paul et al. [18] performed several elastic–plastic finite element analyses to determine crack-opening characteristics for circumferential TWC pipes under pure bending. The experimental data used for validation of finite element results were in the form of COD measurements made during two pipe fracture tests previously conducted at Battelle. One of these experiments, conducted on a 406 mm (16 in.) nominal diameter TP304 stainless-steel unwelded pipe at room temperature (Experiment 8T), was part of an EPRI-funded effort [19]. The data for the other experiment, conducted on a 406 mm (16 in.) nominal diameter TP304 stainless-steel welded pipe at 288°C (550°F) (Experiment 4141-3), was developed from an NRC-sponsored program [13]. During Phase 1 of the IPIRG Program [14], these two experiments were analyzed by elastic–plastic finite element analyses by Paul et al. [18] The results showed that the elastic–plastic FEM can provide accurate estimates of crack-opening displacements and shapes when compared with the corresponding experimental data.

2.2. New thick-walled pipe analysis

During the present study, a full three-dimensional finite element analysis was conducted to predict crack-opening displacement in a through-wall-cracked pipe under pure bending loads [20]. The data used to verify the finite element predictions were obtained from Experiment 1.1.1.21 and were developed in the Short Cracks in Piping and Piping Welds Program [16]. This experiment was conducted on a 711.2-mm (28-in.) nominal diameter Schedule 60 A515 Grade 60 carbon steel unwelded pipe with a short circumferential through-wall crack which has length equal to 6.25% of the pipe circumference. Such crack lengths are typical in LBB applications for larger diameter pipes. Fig. 1 shows the longitudinal dimensions of the pipe sections used to make up the specimen for Experiment 1.1.1.21. Fig. 2 shows the cross-sectional geometry in the cracked section and instrumentation for collecting experimental data.

A three-dimensional elastic–plastic finite element model was developed for this pipe and is shown in Fig. 3. The finite element model consisted of a 1/4 symmetric portion of the

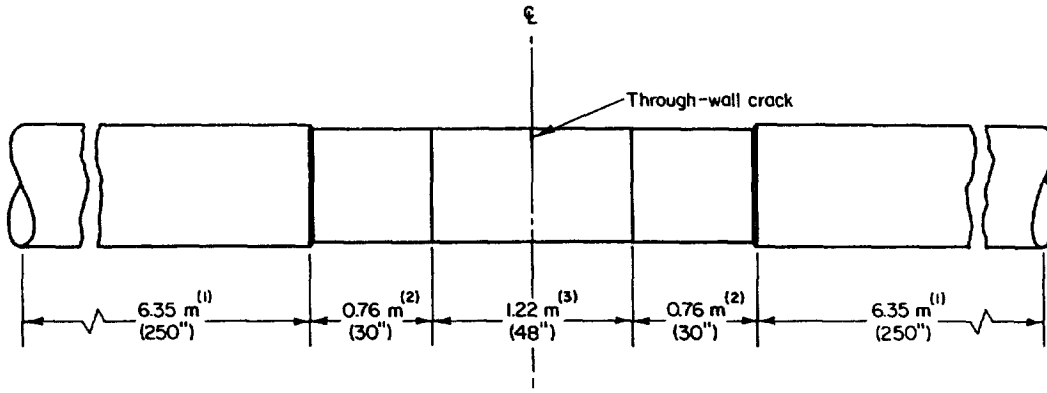

	(1)	(2)	(3)
Diameter	760 mm (30")	711 mm (28")	711 mm (28")
Wall Thickness	38.1 mm (1.5")	25.3 mm (0.995")	22.7 mm (0.893")
Ident. No.	IP-F5	DP2-F90	DP2-F26

Fig. 1. Pipe geometry in Experiment 1.1.1.21.

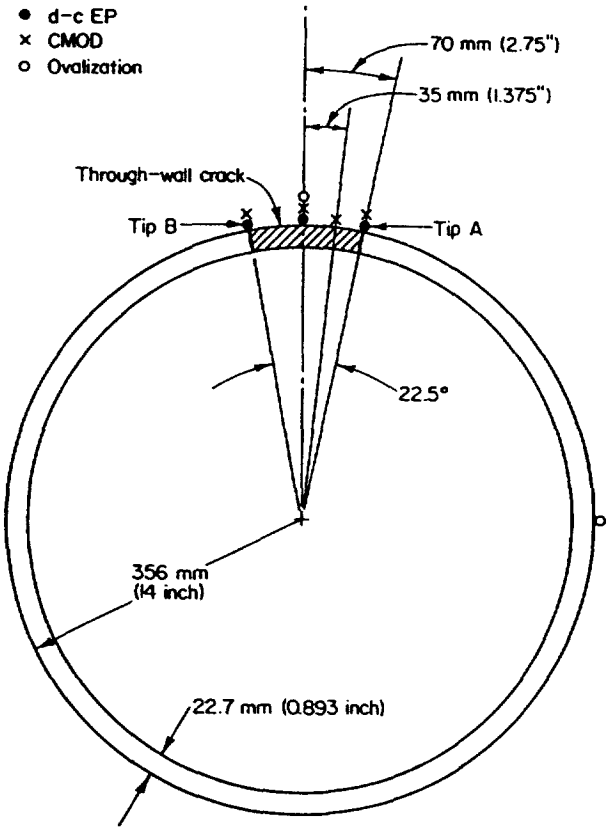

Fig. 2. Crack geometry and instrumentation for Experiment 1.1.1.21.

pipe with three different cross-sections. It consisted of 579 elements and 3761 nodes. The number of elements through the thickness was one. The finite element analysis was performed under displacement control to a maximum

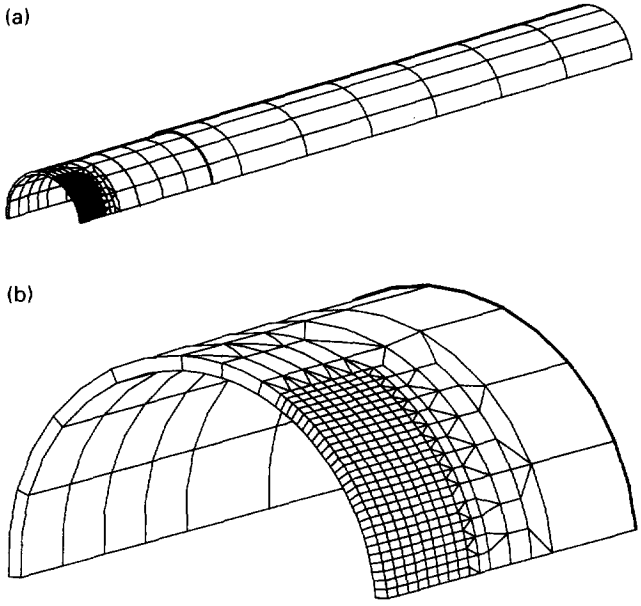

Fig. 3. Finite element model for Experiment 1.1.1.21: (a) finite element mesh for a quarter pipe; and (b) crack-tip mesh refinement.

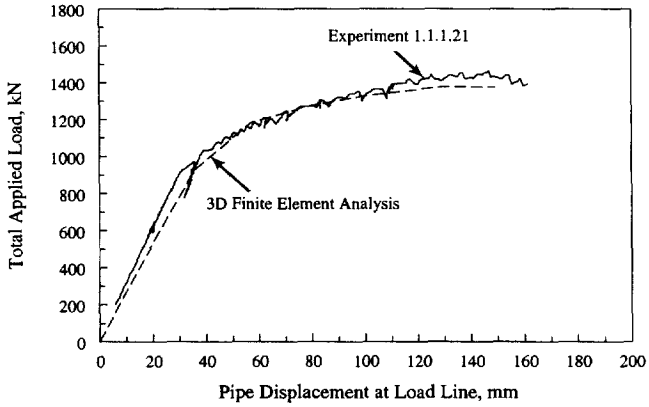

Fig. 4. Load vs displacement comparison for Experiment 1.1.1.21.

load-line displacement of 160 mm (6.3 in.). Based on the experimental data, the crack initiated at a load-line displacement of 62.5 mm (2.46 in.).

Crack growth calculations were performed using the ABAQUS (Version 5.3) finite element code [21] with several load steps. The first load step was up to crack initiation. Subsequent steps consisted of releasing appropriate crack front nodes while simultaneously increasing the load-line displacement. The crack-growth and applied displacement data were obtained from the experimental record. Hence, the finite element predictions of crack-opening displacement following crack initiation were based on crack growth data from the test. As an alternative, the crack growth criteria based on J-integral evaluations could have been used [1], but were not adopted in this particular analysis.

Fig. 4 shows the plots of total load vs pipe displacement at the load line from the experiment and the three-dimensional finite element calculations. The analysis results compare very well with the experimental data. The predicted results of center-crack-opening displacement vs applied loads are shown in Fig. 5. The calculated center CODs presented in this figure were obtained at the outer surface of the pipe. Once again, the agreement between the finite element

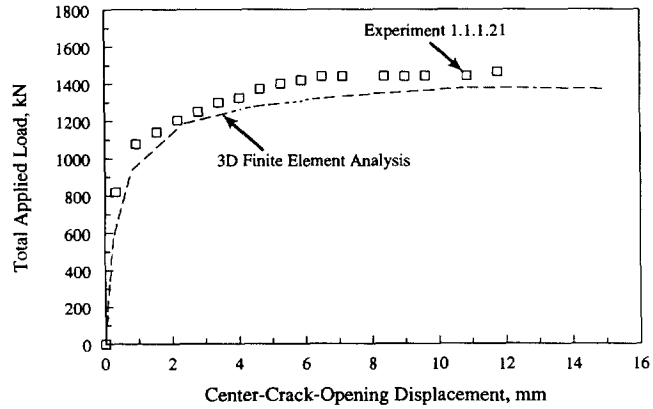

Fig. 5. Comparison of predicted load vs center-crack-opening displacement for Experiment 1.1.1.21.

results and the experimental data from the pipe fracture test is very good.

3. Experimiental verification of estimation models

A total of 25 full-scale pipe fracture experiments were analyzed to determine the predictive capability of the COA estimation models discussed in Rahman et al. [1]. In all of these experiments, the pipes had circumferential through-wall cracks. Two cases of crack geometry were considered. One was a simple through-wall crack which has the same crack length on the inside and outside pipe diameter in terms of percentage of pipe circumference. The other was a complex crack which consists of a 360° internal surface crack that penetrates the pipe thickness for a shorter through-wall-crack length. See Fig. 6 for the definitions of these two crack geometries and the associated crack-size parameters.

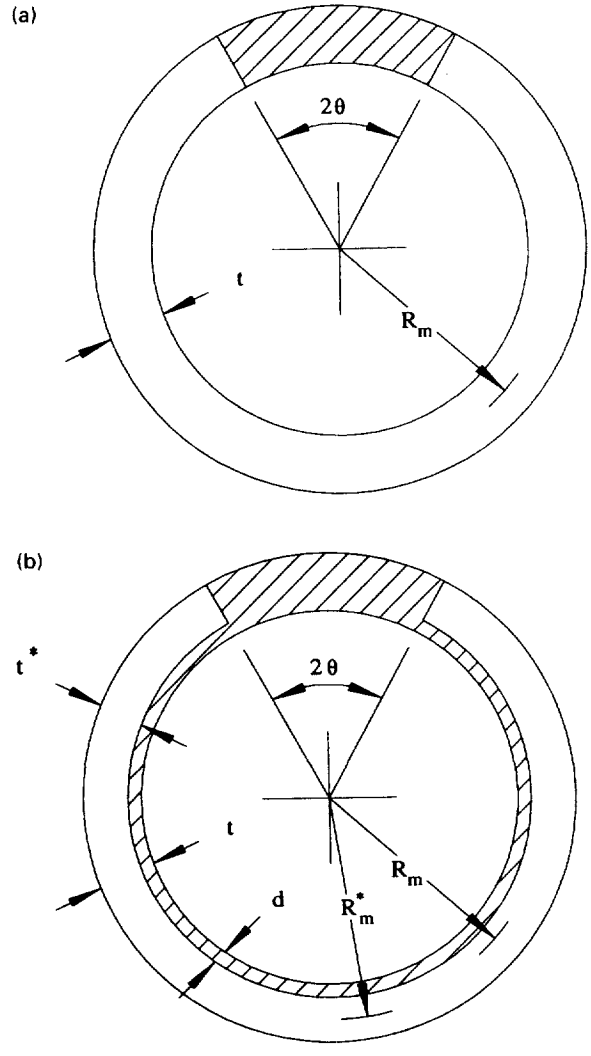

Fig. 6. Various through-wall-crack geometries and definitions of their parameters: (a) simple through-wall crack; and (b) complex crack.

The experiments involved both austenitic and ferritic steel piping with cracks located in the base metal, the weld metal and the bimetallic weld. A wide range of pipe (outer) diameters from 114.3 mm (4.5 in.) to 1067 mm (42 in.) was considered. The initial through-wall crack lengths were both short and long and ranged between 6.25 and 38.6% of the pipe circumference. For the pipes with complex-crack geometry, the 360° internal surface cracks were both shallow and deep and the depths of these cracks varied from 32 to 64% of the pipe thickness. In all experiments, the cracks were placed in the center of the bending plane. For the welded pipe tests, the cracks were located in the center of the weld, except for the bimetallic pipe weld test in which case the crack was placed along the fusion line between the ferritic base metal and Inconel weld metal (see details in Section 3.5). The test temperature varied from 7°C (45°F) to 288°C (550°F) with one experiment at 7°C (45°F), one experiment at room temperature [21°C (70°F)] and the rest of the experiments at 288°C (550°F). The loading conditions were pure bending, pure tension and combined bending and tension. Table 1 shows the summary of pipe fracture experiments analyzed in this study. Fig. 7 shows a schematic of the experimental setup for one of these full-scale pipe fracture tests.

In all of the above pipe experiments, the loading rates were quasi-static. Hence, all material property data used in the analyses were also based on quasi-static loading rates. The applied loads in the experiments were increased monotonically until the failure condition was reached.

3.1. Adequacy of power law ideaiizations for material properties

In the estimation schemes for the COA analysis, the Ramberg–Osgood material model defined in the companion paper [1] (Eq. 1 of Rahman et al. [1]) is necessary since the formulations of crack-opening displacement and other relevant fracture parameters are based on power-law idealization of the stress–strain curve. Unfortunately, there are actual material data for which it can be difficult sometime to represent the complete range of actual stress–strain relationship by a Ramberg–Osgood model.

Brust [7] provides some discussions on the limitation of this material model. It was indicated in this reference and Paul et al. [18] that proper care must be taken in selecting the appropriate range of stress–strain data for a least-squares fit by this power-law model. For typical LBB evaluations of large-diameter pipe, the fracture behavior of a cracked pipe is significantly elastic with little nonlinearity under normal operating conditions, and hence the estimations of crack-opening area and leak rate should be based on a power-law fit for low strain regions. However, for LBB applications involving small-diameter pipes, higher operating stresses, etc., or general pipe flaw evaluations, if the magnitude of nonlinearity is high, the power-law fit to the high-strain region would be more

Table 1
A list of 25 quasi-static pipe experiments for crack-opening-area analysis

Pipe test no.	Outer diameter (mm)	Schedule	Material	Temperature (°C)	Flaw Shape*	$2a/\pi D_m$†	d/t‡	Loading condition§	Reference
			(a) Pipe experiments with base-metal cracks (19 experiments)						
1.1.1.21	711	60	A515 Gr. 60	288	TWC	0.0625	0	B	16
1.1.1.26	106	160	TP316L	21	TWC	0.244	0	B	16
4111-1	114	80	A333 Gr. 6	288	TWC	0.370	0	B	13
4111-2	711	60	A515 Gr. 60	288	TWC	0.370	0	B	13
4111-3	1067	NA¶	TP304	7	TWC	0.370	0	B	13
4121-1	168	120	TP304	288	TWC	0.386	0	T	13
4131-1	166	120	TP304	288	TWC	0.370	0	B + T	13
4131-3	274	100	A333 Gr. 6	288	TWC	0.370	0	B + T	13
1-8	399	100	A106 Gr. B	288	TWC	0.120	0	B + T	—‖
4113-1	168	120	TP304	288	CC	0.370	0.32	B	13
4113-2	168	120	TP304	288	CC	0.370	0.63	B	13
4113-3	168	80	Inconel 600	288	CC	0.370	0.34	B	13
4113-4	168	80	Inconel 600	288	CC	0.370	0.61	B	13
4113-5	168	120	A106 Gr. B	288	CC	0.370	0.31	B	13
4113-6	168	120	A106 Gr. B	288	CC	0.370	0.64	B	13
4114-1	165	120	A106 Gr. B	288	CC	0.370	0.47	B	13
4114-2	166	120	TP304	288	CC	0.370	0.32	B	13
4114-3	413	100	TP304	288	CC	0.373	0.34	B	13
4114-4	413	100	TP304	288	CC	0.373	0.34	B	13
			(b) Welded pipe experiments (5 experiments)|					
1.1.1.23	711	80	TP316L SAW	288	TWC	0.0625	0	B	16
1.1.1.24	612	80	A333 Gr. 6 SAW	288	TWC	0.079	0	B	16
4141-1	168	120	TP304 SAW	288	TWC	0.371	0	B	13
4141-5	168	120	TP304 SA-SAW	288	TWC	0.383	0	B	13
4111-5	720	80	TP316 SMAW	288	TWC	0.370	0	B	13
			(c) Bimetallic pipe weld experiment (1 experiment)|					
1.1.1.28	930	160	A516 Gr. 70/F316/ Inconel 182 SMAW	288	TWC	0.359	0	B	16

*TWC = simple through-wall crack; CC = complex crack.
†$2a$ = through-wall crack length at mean pipe diameter; D_m = mean pipe diameter.
‡d = depth of 360° internal surface crack in a complex-cracked pipe; t = pipe wall thickness.
§B = pure bending; T = pure tension (pressure); B + T = combined bending and tension (pressure).
¶Not applicable.
‖Data were developed in the IPIRG-2 Program at Battelle.
|SAW = submerged-arc weld; SMAW = shielded-metal arc weld; SA-SAW = solution-annealed submerged-arc weld.

appropriate. Since this study is focused on evaluating crack-opening characteristics up to initiation load or maximum load that are usually associated with large plastic strains, the Ramberg–Osgood fit in the high-strain region was used to determine the model parameters, α and n. From our past experience, we found that the range of raw stress–strain data between 1% strain and 80% of ultimate strain would provide the best representation by the Ramberg–Osgood model when analysing pipe fracture experiments. All values of α and n presented in this study were computed in this strain range. Quantitative details on how α and n are affected by the choice of strain range and their impact on COA predictions are given in a topical report from this study [20].

In characterizing the fracture toughness of materials, the ASTM deformation J-resistance curve (the J_D–R curve) was used for pipes with simple through-wall cracks. For pipes with complex cracks, the modified J-resistance curves (J_M–R curves) were used. For most of these cases, the J_D–R curve and J_M–R curves were extrapolated by either a power-law hardening model [i.e. Eq. (2) of Rahman et al. [1]] and a linear model [i.e. a special case of $m = 1$ in Eq. (2) in the aforementioned reference], respectively, for crack growth beyond 30% of the uncracked ligament in the compact ension [$C(T)$] specimens [13–16]. Because, the $C(T)$ specimens were small, large extrapolation of the data was necessary in order to predict crack growth in a pipe. Since, in many cases, there were more than one set of experimental data for both stress–strain and J–R curves, the values of material property constants presented and used in the analyses represent their average values.

3.2. The NRCPIPE computer program

The NRCPIPE computer code was developed to perform elastic–plastic fracture-mechanics analysis for establishing the fracture-failure conditions of a piping system in terms

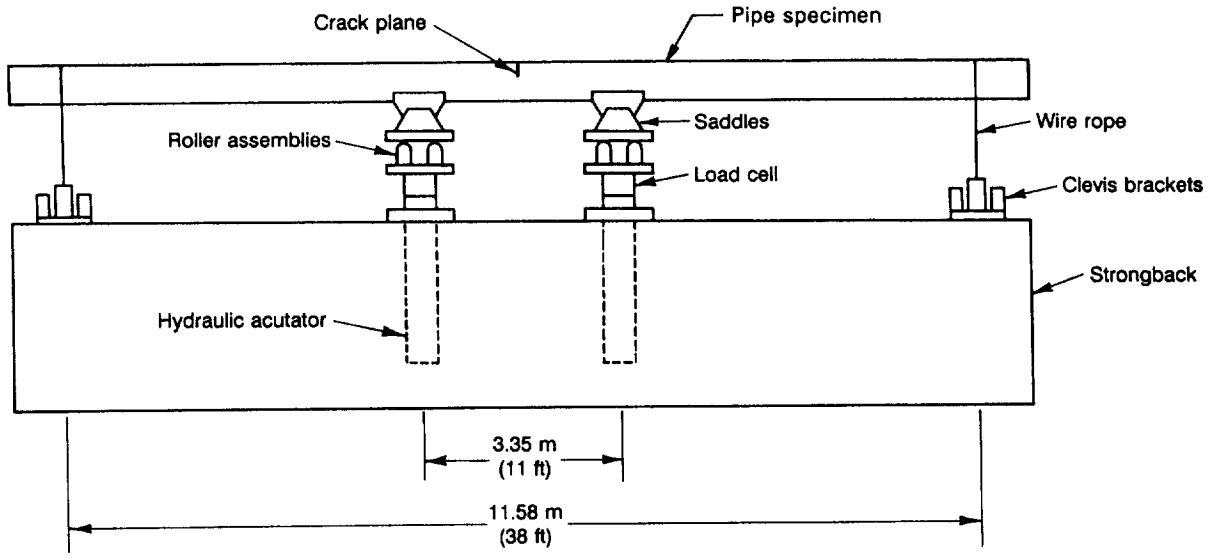

Fig. 7. Schematic of experimental setup for Experiment 1.1.1.23.

of sustainable load (or stress) or displacement [16]. For nuclear applications, engineering elastic–plastic fracture-mechanics techniques are based on the J-integral fracture parameter. To perform a fracture analysis, the user provides the input data describing the pipe and crack geometries, material stress–strain characteristics and fracture resistance of the material (i.e. a J–R curve) as obtained from a laboratory test specimen. A wide variety of results for a pipe including crack-opening area predictions can be obtained from this program.

The use of elastic–plastic fracture mechanics to predict crack-opening area in TWC pipes was studied by various researchers [1–12]. Although a number of procedures were proposed, there is little experimental validation. For this reason, the NRCPIPE code was written to include numerous analysis procedures. At the user's option, NRCPIPE can perform an analysis using any of these procedures. In addition, the modular structure of NRCPIPE permits inclusion of new procedures as they are developed.

The NRCPIPE code was originally developed under the Degraded Piping Program [13]. A significant amount of development and numerous enhancements was made in the Short Cracks in Piping and Piping Welds Program [16]. Further details on these enhancements can be obtained from this reference [16].

The pipe fracture experiments listed in Table 1 were analyzed by various estimation methods described earlier. All of these methods are available in the current version of the NRCPIPE code (Version 2.0). All crack-opening results for the analyses of these experiments were generated using this program. The results are discussed in Sections 3.3, 3.4 and 3.5.

3.3. Analysis of pipes with base metal cracks

This section discusses the crack-opening-area analyses of 19 pipe fracture experiments involving nine through-wall-cracked pipes and 10 complex-cracked pipes. Five of these TWC pipe tests, such as Experiments 1.1.1.21, 1.1.1.26, 4111-1, 4111-2, 4111-3, were performed at pure bending load without any internal pressure. Experiment 4121-1 was conducted under a pure tension load due to internal pipe pressure. The remaining three TWC pipe tests, Experiments 4131-1, 4131-3 and 1-8, were performed under combined bending and tension due to constant pipe pressure. On the other hand, all of the 10 complex-cracked pipes tested in Experiments 4113-1 to 4113-6 and 4114-1 to 4114-4 were subjected to pure bending without internal pressure. The fracture data for these experiments were developed during the Short Cracks in Piping and Piping Welds Program [16] the Degraded Piping Program [13] the Second International Piping Integrity Research Group (IPIRG-2) Program [15]. Table 2 provides a summary of the pipe geometries and experimental results for these 19 pipe fracture experiments. Material properties, including the power-law fit parameters for the stress–strain curves and the $C(T)$ specimen J–R curves related to these experiments, are given in Table 3.

3.3.1. Simple through-wall-cracked pipes

Figs. 8(a)–10(a) show the plots of total applied load (in four-point bending) vs center-crack-opening displacement for the nine through-wall-cracked pipes with base-metal cracks from Experiments 1.1.1.21, 1.1.1.26, 4111-1, 4111-2, 4111-3, 4121-1, 4131-1, 4131-3 and 1-8, respectively. These plots were developed from both predictive formulas by several estimation models and experimental pipe fracture data mentioned previously.

3.3.1.1. Pure bending. The results in Figs. 8(a)–Fig. 9(a) involving only pure bending loads indicate that the LBB.ENG2 method provides excellent predictions of experimental COD. The only exception is Experiment 1.1.1.21. The crack size in Experiment 1.1.1.21 was very

Table 2
Summary of pipe geometry and results for 19 pipe fracture experiments with base-metal cracks

Pipe test no.	Outer diameter (mm)	Pipe thickness (mm)	Pipe material	Internal pressure (MPa)	$2a/\pi D_m$*	d/t†	Inner span (m)	Outer span (m)	Initiation load (kN)	Maximum load (kN)
(a) Through-wall-cracked pipes (nine experiments)										
1.1.1.21	711	22.70	A515 Gr. 60	0	0.0625	0	3.35	11.58	1250	1470
1.1.1.26	106	8.31	TP316L	0	0.244	0	0.61	1.52	73	75
4111-1	114	8.89	A333 Gr. 6	0	0.370	0	0.81	1.52	73	88
4111-2	711	23.62	A515 Gr. 60	0	0.370	0	3.35	11.58	396	585
4111-3	1067	7.11	TP304	0	0.370	0	3.35	11.58	299	443
4121-1	168	12.88	TP304	—‡	0.386	0	NA§	NA§	—¶	—‖
4131-1	166	13.41	TP304	17.24	0.370	0	1.22	3.2	31	40
4131-3	274	18.69	A333 Gr. 6	12.45	0.370	0	3.35	7.92	70	100
1-8	399	26.20	A106 Gr. B	15.51	0.120	0	3.35	11.58	302	504
(b) Complex-cracked pipes (10 experiments)										
4113-1	168	14.48	TP304	0	0.370	0.32	0.61	1.52	110	124
4113-2	168	14.48	TP304	0	0.370	0.63	0.61	1.52	76	81
4113-3	168	11.05	Inconel 600	0	0.370	0.34	0.61	1.52	106	118
4113-4	168	11.05	Inconel 600	0	0.370	0.61	0.61	1.52	79	87
4113-5	168	14.22	A106 Gr. B	0	0.370	0.31	0.61	1.52	118	147
4113-6	168	14.22	A106 Gr. B	0	0.370	0.64	0.61	1.52	55	89
4114-1	165	12.73	A106 Gr. B	0	0.370	0.47	1.22	2.34	68	83
4114-2	166	13.46	TP304	0	0.370	0.32	1.22	4.17	26	29
4114-3	413	26.16	TP304	0	0.373	0.34	3.35	11.58	146	158
4114-4	413	26.16	TP304	0	0.373	0.34	3.35	11.58	141	152

*$2a$ = through-wall crack length at mean pipe diameter; D_m mean pipe diameter.
†d = depth of 360° internal surface crack in a complex-cracked pipe; t = pipe wall thickness.
‡Pressure monotonically increased until failure.
§Not applicable.
¶The initiation pressure was 26.9 MPa (3.9 ksi).
‖The maximum pressure was 30.1 MPa (4.4 ksi).

short ($2a/\pi D_m$ = 6.25%) and it appears that for this experiment, the GE/EPRI method using either the original or the newly-developed influence functions from this study can predict COD with better accuracy than the other methods, at least up to crack initiation [Note, the measured initiation load for Experiment 1.1.1.21 was 1250 kN (281 013 lb)]. In Experiments 1.1.1.21 and 1.1.1.26, both the LBB.NRC and Paris/Tada methods underpredicted COD for applied loads that are less than the initiation load, although the results from the LBB.NRC method were closer to the experimental data. In Experiments 4111-1 to 4111-3, the CODs predicted by the LBB.ENG2 method and the GE/EPRI method (using original functions) were very similar and compared very well with the experimental data.

3.3.1.2. Pure tension. Fig. 9(b) shows the plots of both predicted and experimental results of applied pipe pressure as a function of center-crack-opening displacement in Experiment 4121-1 conducted under pure tension load (pressure induced). The GE/EPRI method (original functions) slightly overestimated both the experimental COD and the predicted COD by the LBB.ENG2 method. The agreement between the results from the LBB.ENG2 method and the experiment was excellent.

3.3.1.3. Combined bending and tension. For the pipe tests, Experments 4131-1, 4131-3 and 1-8 that involved combined bending and tension (pressure induced), similar plots of load vs center COD were developed and are shown in Fig. 9(c and d) and Fig. 10(a), respectively. In these experiments, the measured COD values due to the initial pipe pressure were initialized before the application of additional bending loads. Hence, the center-crack-opening displacement plotted in these figures is equal to the center COD under combined bending and tension loads minus the center COD due to the pure tension load before the bending loads are applied.

For Experiment 4131-1 [see Fig. 9(c)], it is seen that all estimation methods underpredicted the COD for applied load before the crack growth initiated. [Note, the measured initiation load for Experiment 4131-1 was 31.00 kN (6969 lb).] The Paris/Tada and LBB.NRC solutions gave the worst predictions, while the LBB.ENG2 and GE/EPRI methods predicted results closer to the experimental data. In Experiment 4131-3 [see Fig. 9(d)], the Paris/Tada and LBB.NRC methods underpredicted COD as in Experiinent 4131-1, but the magnitude of underprediction by the LBB.NRC method was much smaller. In fact, for this particular experiment, the LBB.NRC method made better predictions of test data than any other methods.

Table 3
Tensile strength and fracture toughness properties of pipe materials for experiments with base-metal cracks

Pipe test no.	Elastic modulus (E) (GPa)	Yield stress (σ_y) (MPa)	Ultimate stress (σ_u) (MPa)	Ramberg–Osgood coefficients*		Extrapolated J–R curve parameters†		
				α	n	J_{Ic} (kJ/m^2)	C (kJ/m^2)	m
1.1.1.21	179.3	231	544	1.10	5.50	207	166	0.483
1.1.1.26	157.5	254	532	5.50	4.76	879	779	0.974
4111-1	179.3	198	494	1.96	4.16	335	—§	—§
4111-2	179.3	231	544	1.10	5.50	207	166	0.483
4111-3	199.9	220	682	1.67	5.05	484	258	0.646
4121-1	179.3	139	450	4.91	3.88	1090	—¶	—¶
4131-1	179.3	139	450	4.91	3.88	1090	—¶	—¶
4131-3	179.3	239	527	3.77	3.84	298	—¶	—¶
1-8	193.1	217	508	174	4.66	72	140	0.72
				(b) Complex-cracked pipes				
4113-1	183.8	139	450	5.33	3.80	1210	328	1
4113-2	183.8	139	450	5.33	3.80	1210	328	1
4113-3	221.4	197	610	5.35	3.90	1820	505	1
4113-4	221.4	197	610	5.35	3.90	1820	505	1
4113-5	198.4	320	621	1.20	5.90	100	107	1
4113-6	198.4	320	621	1.20	5.90	100	107	1
4114-1	198.4	320	621	1.20	5.90	100	107	1
4114-2	183.8	139	450	5.33	3.80	1210	328	1
4114-3	179.5	186	461	2.83	5.50	310	167	1
4114-4	179.5	186	461	2.83	5.50	310	167	1

*Stress–strain curve is represented by: $\epsilon/\epsilon_0 = \sigma/\sigma_0 + \alpha(\sigma/\sigma_0)^n$ where $\sigma_0 = \sigma_y$, $\epsilon_0 = \sigma_0/E$.
†For through-wall-cracked pipe, the J_D–R curve was used and was represented by: $J = J_{Ic} + C(\Delta a/r)^m$ and where $r = 1$ mm and Δa is in millimeters.
‡For a complex-cracked pipe, the J_M–R curve was used and was represented by: $J = J_{Ic} + C\,\Delta a$, where Δa is in millimeters.
§Crack growth data were not available.
¶Actual J_D–R data from $C(T)$ specimens were used which were extrapolated linearly at the last two points.

Fig. 10(a) shows the results of Experiment 1-8 that has a crack length of only 12% of the pipe circumference. For this experiment, the LBB.ENG2 method provided good predictions of COD for smaller loads, but also underpredicted COD significantly for larger loads. The trend curves for the Paris/Tada and LBB.NRC methods showed similar behavior in predicting COD. Among all of these methods, the GE/EPRI method without plastic-zone correction (PZC) using either the original or the newly-developed influence functions provided the best results. Similar observations were also made for a pure bending pipe Experiment 1.1.1.21 with short cracks, see Fig. 8(a).

3.3.2. Complex-cracked pipes

A complex crack is a very long, internal surface crack in a pipe, which may penetrate the wall thickness, thereby creating a short through-wall crack in the same plane as the surface crack [see Fig. 6(b)]. A detailed numerical investigation of the complex-cracked pipe problem using three-dimensional finite element nonlinear analysis can be prohibitively expensive and was considered beyond the scope of the current effort. Instead, simple engineering estimation techniques were used. It was assumed that the available estimation formulas for simple through-wall circumferentially cracked pipes that were discussed in Rahman et al. [1] could be applied to analyze complex-cracked pipes. This was performed by adjusting the pipe radius (e.g. adjusted radius, $R^* = R_m + d/2$) and the thickness (e.g. adjusted thickness, $t^* = t - d$) in the cracked plane to account for the presence of the surface crack. Thus, any radial crack-driving force contribution was ignored. Only growth of the through-wall crack in the circumferential direction was considered. In addition, possible closure of the surface crack in the compressively stressed region of the crack plane was not included in the analysis, which can cause the loads to be underpredicted and the crack-opening to be overpredicted.

Figs. 10(b)–12(c) show the plots of total load vs center-crack-opening displacement for the 10 complex-cracked pipes with base-metal cracks from Experiments 4113-1 to 4113-6 and 4114-1 to 4114-4, all of which were performed under four-point bending without any internal pressure. These plots contain results from the analyses by the LBB.ENG2 method (only) and the corresponding experimental data. The results suggest that in most cases, the exceptions being Experiments 4113-5, 4114-1 and 4114-2, this estimation model (LBB.ENG2 method) overestimates the COD at all load levels. This can be qualitatively explained by noting that for a complex-cracked pipe, an effective pipe thickness, $t^* = t - d$ was used in the estimation formulas for simple through-wall-cracked pipes. Consequently, the 'equivalent' through-wall-cracked pipe

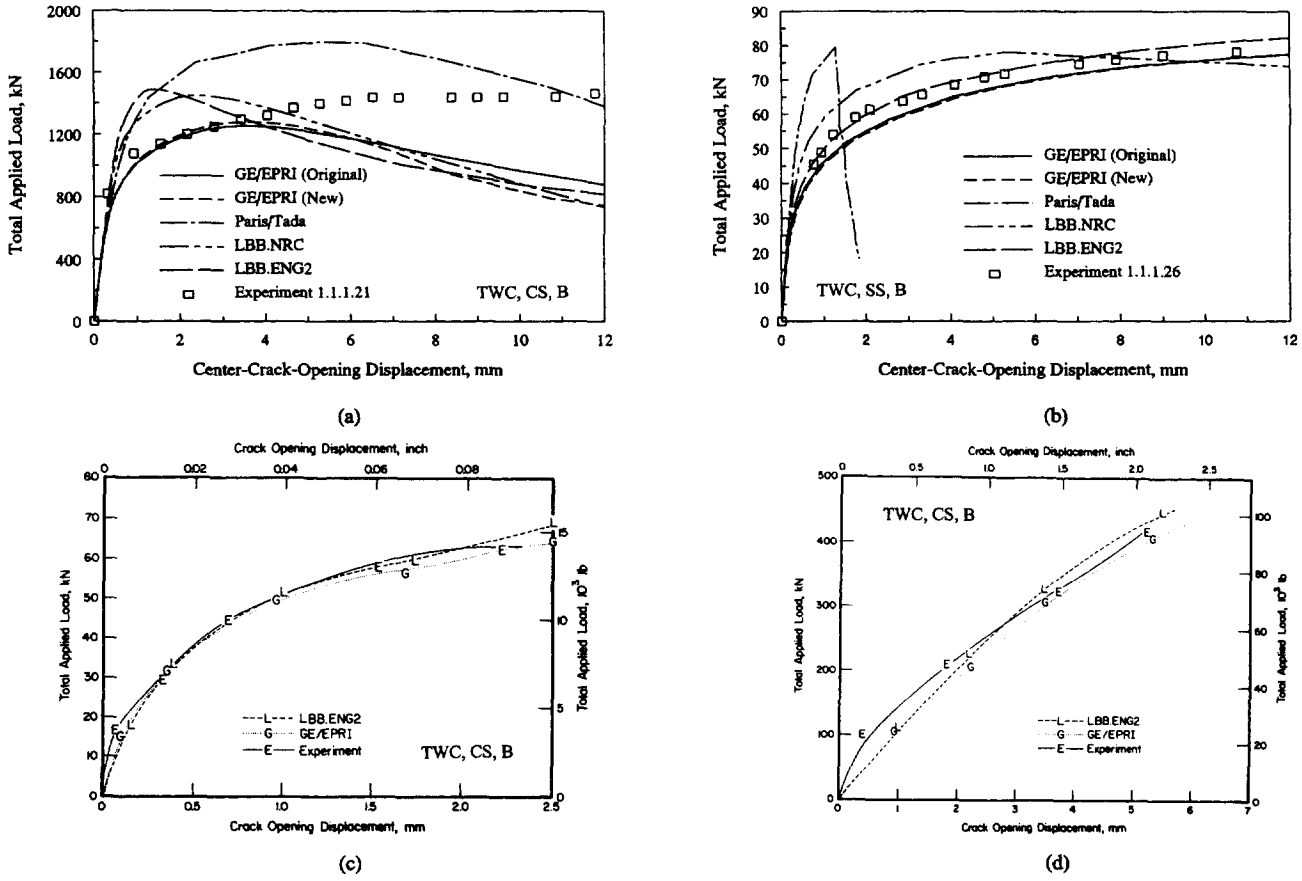

Fig. 8. Load vs center-crack-opening displacement in: (a) Experiment 1.1.1.21; (b) Experiment 1.1.1.26; (c) Experiment 4111-1; and (d) Experiment 4111-2.

assumed in an estimation model would have lower stiffness than the actual complex-cracked pipe. Hence, the predicted crack-opening displacements were larger than the experimental results. Obviously, when the surface cracks become deeper (e.g. Experiments 4113-2, 4113-4 and 4113-6), the magnitudes of these overestimates of the COD will also become larger and can be significantly different from the experimental results, as exhibited in Fig. 10(c), Fig. 11(a) and Fig. 11(c). Again, this general loss of accuracy can be attributed to the over-simplification in the estimation formulas for through-wall-cracked pipes used for predicting the COD of complex-cracked pipes. Clearly, further studies are needed to develop accurate COA models for complex-cracked pipe.

3.4. Welded pipe analysis

In this section, the results of crack-opening-area analyses of five pipe fracture experiments on through-wall-cracked pipes with the cracks in welds are presented. The pipe tests are Experiments 1.1.1.23, 1.1.1.24, 4141-1, 4141-5 and 4111-5, all of which were performed at pure bending without any internal pressure. The materials in the Experiments 1.1.1.23 and 1.1.1.24 were TP3 16L stainless-steel submerged-arc weld (SAW) and A333 Grade 6 submerged-arc weld, respectively. The crack lengths in Experiments 1.1.1.23 and 1.1.1.24 were short and were 6.25 and 7.9% of the pipe circumference, respectively. The fracture data for these two experiments were developed in the Short Cracks in Piping and Piping Welds Program [16]. In Experiments 4141-1 and 4141-5, the materials were TP304 stainless-steel submerged-arc weld. However, the weld in Experiment 4141-5 was solution-annealed to eliminate the residual stresses. The material for Experiment 4111-5 was TP316L shielded-metal arc weld (SMAW). The crack lengths in Experiments 4141-1, 4141-5 and 4111-5 were long and were 37.1, 38.3 and 37% of the pipe circumference, respectively. The fracture data for these three experiments were developed in the Degraded Piping Program [13].

Table 4 shows a summary of the pipe geometries and test results for these five experiments on welded pipes. Tensile strength properties of the materials, including the power-law fit parameters for both base and weld metals, are provided in Table 5. The fracture toughness properties of the welds in terms of power-law parameters are given in Table 6.

Figs. 12(d)–Fig. 13(d) show the comparisons of predicted load vs COD results with experimental data from the above pipe tests. A wide variety of estimation models were used to perform such comparisons. In Experiment 1.1.1.23 ($2a/\pi D_m$ = 6.25%), the Paris/Tada, the LBB.NRC, the LBB.ENG2 and the LBB.ENG3 methods underpredicted the experimental COD for most of the load ranges. The

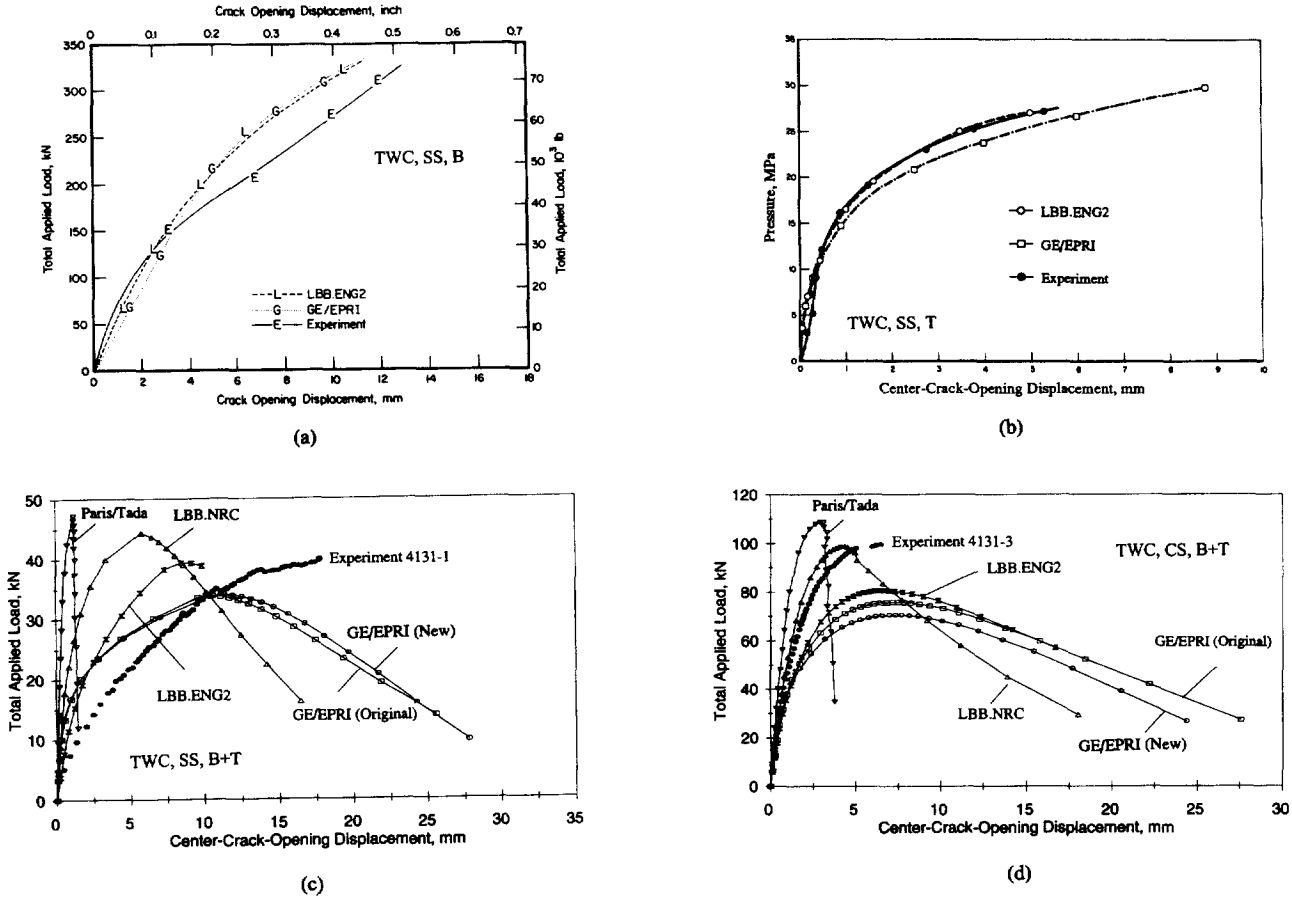

Fig. 9. Load vs center-crack-opening displacement in: (a) Experiment 4111-3; (b) Experiment 4121-1; (c) Experiment 4131-1; and (d) Experiment 4131-3.

GE/EPRI methods with the original and the newly-developed influence functions overpredicted the COD significantly at both small and large load levels. In Experiment 1.1.1.24 ($2a/\pi D_m = 7.9\%$), all of the estimation methods, except the GE/EPRI method, underpredicted experimental results for most of the load ranges as also observed for Experiment 1.1.1.21 with a base-metal crack. However, for this experiment, the agreement between the predicted results from the GE/EPRI method and experimental data was very good up to initiation load. [Note, the measured initiation load for the Experiment 1.1.1.24 was 1110 kN (249 500 lb).]

In Experiments 4141-1, 4141-5 and 4111-5, all of which have long cracks, the comparisons of the predicted load vs COD relationship with experimental data show mixed trends. The predicted results for Experiments 4141-1 and 4141-5 [see Fig. 13(b and c)] are consistent in the sense that most estimation methods overpredicted COD except the Paris/Tada method, which exhibited almost linear (and stiff) behavior, thus significantly underpredicting crack-opening for a given load. For Experiment 4111-5 [see Fig. 13(d)], all methods underpredicted COD for most of the load ranges. Among the predictive schemes, the LBB.ENG2 and GE/EPRI methods produced results closer to the experimental data.

3.4.1. J_D–R curves from pipes and $C(T)$ specimens for experiments 4141-1 and 4141-5

In order to explain why there was so much underprediction in loads for the Experiments 4141-1 and 4141-5, several η-factor analyses were conducted to generate pipe J_D–R curves using load–displacement records from the actual pipe experiments [22–23]. The objective was to determine the adequacy of J_D–R curves from 1T $C(T)$ specimens used in the analyses of these experiments. Further details on the η-factor analysis can be found in Wilkowski et al. [22].

Fig. 14 shows the comparisons of both as-welded (Experiment 4141-1) and solution-annealed (Experiment 4141-5) SAW J–R curves obtained from 1T $C(T)$ specimens and 152.4-mm (6-in.) diameter pipes via η-factor analyses. Two points are worthy of discussion regarding the SAW pipe data. First, the J_D–R curves from both pipe experiments were greater than those from the $C(T)$ specimens. This is believed to be mainly due to the effects of the weld thickness and weld procedure. For instance, the 1T $C(T)$ specimens were 25.4 mm (1 in.) thick. The 152.4-mm (6-in.) nominal diameter pipes, however, were 14.3 mm (0.562 in.) or 14.1 mm (0.555 in.) thick. The weld procedure involved depositing two layers using the tungsten inert-gas (TIG) weld process, then depositing two layers using the

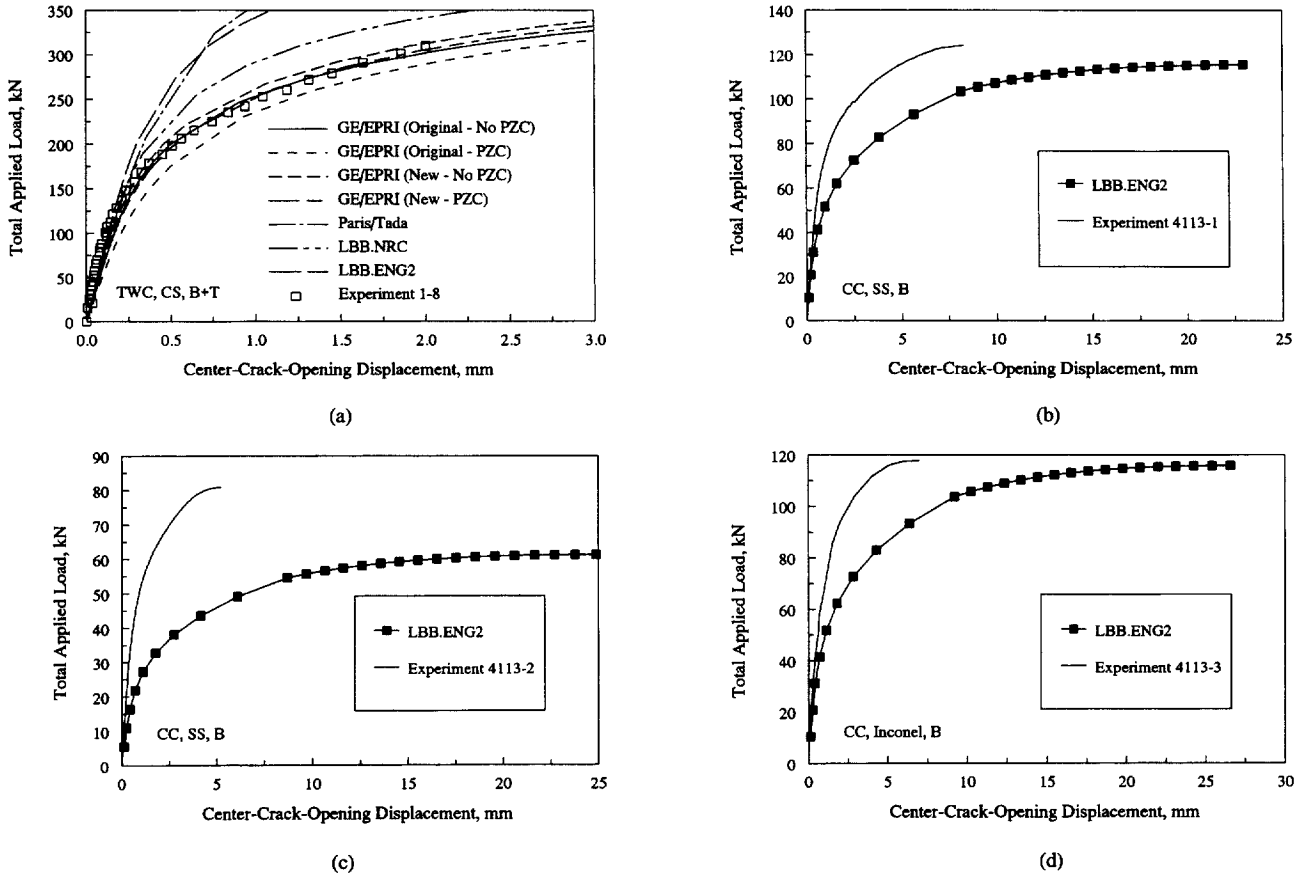

Fig. 10. Load vs center-crack-opening displacement in: (a) Experiment 1-8; (b) Experiment 4113-1; (c) Experiment 4113-2; and (d) Experiment 4113-3.

SMAW process, with the remainder of the weld joint filled using the SAW process. Hence with the thinner pipes, the amount of SAW metal was significantly less than in the 25.4-mm (1-in.) thick weldments of 1*T* *C*(*T*) specimens. Since the TIG weld metal is much higher in toughness, [22] the composite toughness of the 152.4-mm (6-in.) diameter pipes with 14.3 mm (0.562 in.) or 14.1 mm (0.555 in.) thickness was much higher. Perhaps this explains why the estimation schemes with the results shown in Fig. 13(b and c) significantly underpredicted the loads and overpredicted the crack-opening.

The other point is that the *J*–*R* curve for the pipe with the SAW that was solution-annealed is lower than the as-welded SAW pipe *J*–*R* curve. This trend is the opposite to the C(T) specimen results (see Fig. 14). For a typical η-factor analysis, the plastic component of the *J*-integral is proportional to the area under the load–displacement record. From Fig. 15, showing the load vs load–point displacement records for the above two experiments, the area under the load–displacement record for as-welded pipe (Experiment 4141-1) is larger than that for solution-annealed pipe (Experiment 4141-5). Hence, the value of the *J*-integral, exhibited in pipe J_D–*R* curves, is higher for the as-welded pipe. Nevertheless, additional *C*(*T*) specimen data for various sizes and thicknesses would be helpful in clarifying this apparent anomaly.

3.4.2. Crack-opening predictions using J_D–R curves from pipes

Following the comparisons between *C*(*T*) and pipe *J*–*R* curves, the estimation analyses were conducted again using the pipe J_D–*R* curves from Fig. 14 to determine the crack-opening displacements for Experiments 4141-1 and 4141-5. The results are shown in Fig. 16(a and b). Predictions made using the pipe, J_D–*R* curves when compared with the experimental results appear to be better than those using *C*(*T*) specimen J_D–*R* curves. Most estimation methods provided reasonably accurate predictions and among the five estimation methods considered here, LBB.ENG3 and LBB.NRC are the most accurate methods for computing crack-opening displacements of as-welded and solution-annealed pipes when the fracture toughness properties are generated from large-scale pipe tests. It appears that when the strength characteristics of weld metal are considered (e.g. in the LBB.ENG3 method), the accuracy of the predictive models can be improved.

3.5. Bimetallic pipe weld analysis

The bimetallic pipe weld in Experiment 1.1.1.28 was part of a 930-mm (36.6-in.) outer diameter, cold-leg piping systems from a cancelled Combustion Engineering nuclear power plant. The welds joined the ferritic cold-leg pipe to

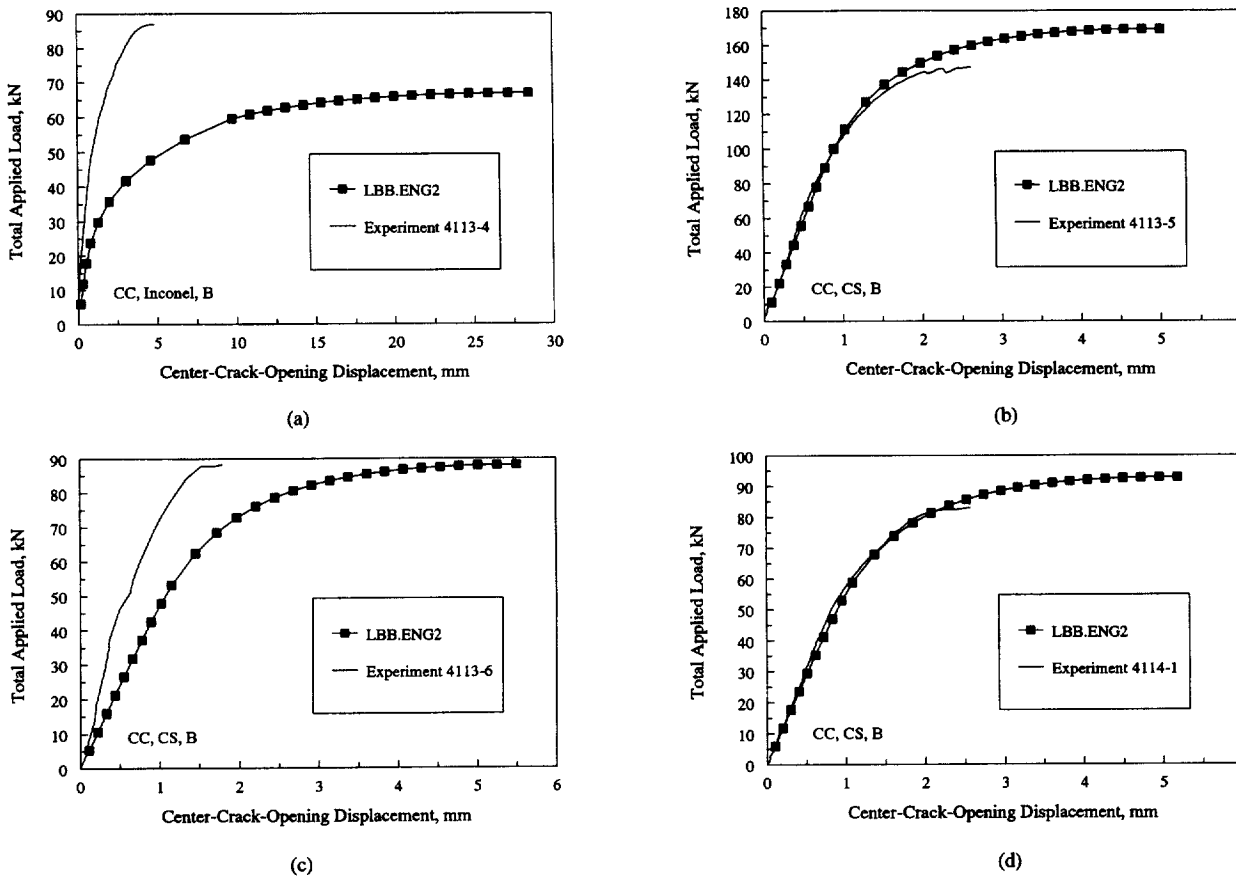

Fig. 11. Load vs center-crack-opening displacement in: (a) Experiment 4113-4; (b) Experiment 4113-5; (c) Experiment 4113-6; and (d) Experiment 4114-1.

stainless-steel safe ends which were to be welded to stainless-steel pump housings. The carbon steel pipe material was A516 Grade 70. The safe ends were fabricated from SA182 F316 stainless-steel (forged TP316 stainless-steel). The welds were fabricated by first buttering the beveled end of the carbon steel pipe with an ENiCrFe-3 (Inconel 182) electrode. The welds joining the buttered pipes and the stainless steel safe ends were then completed using a shielded-metal-arc weld process, using an Inconel 182 weld rod.

The pipe in Experiment 1.1.1.28 had a wall thickness of 81.3 mm (3.20 in.). A through-wall-crack, with length 35.9% of pipe circumference, was placed at the interface between the buttered A516 Grade 70 carbon steel pipe and the Inconel 182 weld. The tensile properties for the A516 Grade 70 carbon steel, SA182 F316 stainless-steel and Inconel 182 weld are given in Table 7. The J–R curve properties for A516 Grade 70 carbon steel, SA182 F316 stainless-steel and A516 Grade 70/Inconel 182 fusion-line region are also given in Table 7.

To determine the crack-opening for the bimetallic weld specimen, three sets of analyses were conducted using the tensile properties of the A516 Grade 70 carbon steel pipe, the SA182 F316 stainless-steel safe end and the Inconel 182 weld. In each set of analyses, the same J–R curve of A516 Grade 70/Inconel 182 Weld fusion-line region was used. A total of five estimation methods were applied to predict the crack-opening displacement for Experiment 1.1.1.28. Fig. 17 shows the comparisons of predicted results in terms of load vs center COD plots with the experimental

Table 4
Summary of pipe geometry and results for five through-wall-cracked welded pipe experiments subjected to pure bending

Pipe test no.	Outer diameter (mm)	Pipe thickness (mm)	Pipe material	$2a/\pi D_m$*	Inner span (m)	Outer span	Initiation load (kN)	Maximum load (kN)
1.1.1.23	711	30.2	TP316L SAW	0.0625	3.35	11.58	1274	1489
1.1.1.24	612	31.3	A333 Gr6 SAW	0.079	3.35	11.58	1110	1660
4141-1	168	14.3	TP304 SAW	0.371	1.20	3.25	58	74
4141-5	168	14.1	TP304 SA-SAW	0.383	1.20	3.25	46	61
4111-5	720	30.2	TP316 SMAW	0.370	3.35	11.58	471	611

*$2a$ = through-wall crack length at mean pipe diameter; D_m = mean pipe diameter.

Table 5
Tensile strength properties of pipe materials for through-wall-cracked welded pipe experiments subjected to pure bending

Pipe test no.	Base metal properties*					Weld metal properties*				
	Elastic modulus (E) (GPa)	Yield stress (σ_y) (MPa)	Ultimate stress (σ_u) (MPa)	α	n	Elastic modulus (E) (GPa)	Yield stress (σ_y) (MPa)	Ultimate stress (σ_u) (MPa)	α	n
1.1.1.23	183	143	427	8.71	3.26	183	366	503	1.63	10.94
1.1.1.24	200	229	525	2.14	4.36	200	412	578	1.41	9.65
4141-1	183	138	449	9.69	3.13	183	324	466	2.28	11.03
4141-5	183	138	449	9.69	3.13	183	194	465	3.42	4.84
4111-5	183	229	501	4.42	4.96	183	282	485	1.84	7.31

*Stress–strain curve is represented by: $\epsilon/\epsilon_0 = \sigma/\sigma_0 + \alpha(\sigma/\sigma_0)^n$, where $\sigma_0 = \sigma_y$, $\epsilon_0 = \sigma_0/E$.

data. The results from these figures suggest that when the tensile properties of SA182 F316 stainless steel and Inconel 182 weld were used, the maximum load from the experiment would be underpredicted (except the Paris/Tada method) and overpredicted, respectively, by the estimation methods considered here. Correspondingly, using the tensile properties of these two materials, the experimental COD for a given applied load would be overpredicted (except the Paris/Tada method) and underpredicted, respectively. However, when the tensile properties of A516 Grade 70 were used, the predicted loads and COD by the estimation methods, particularly by the LBB.ENG2 and the GE/EPRI methods, were in good agreement with the corresponding experimental data. Further details on fracture analysis with explicit predictions of initiation and maximum loads including the ASME Section XI flaw evaluation for this bimetallic-weld pipe experiment are published in a separate topical report [24].

4. Performance evaluation of predictive analyses

4.1. Crack-opening predictions for typical LBB applications

In general, for LBB applications, one is more interested in the accuracy of the models in the elastic load range than at crack initiation load, maximum load, or beyond maximum load. Since stresses in LBB or leak-rate analyses for piping under normal operating loads are generally thought to be in the elastic range, we have statistically qualified the accuracy of the various methods in this region. To simplify this evaluation, we defined the linear–elastic region to occur when the applied load was 40% of the maximum experimental load or less. According to the ASTM guidelines for J–R curve testing, 40 and 50% of the limit load using yield strength as the collapse stress are currently used for fatigue precracking of $C(T)$ and bend specimens [25]. Hence, at 40% of the maximum experimental load, the cracked pipes should experience primarily linear–elastic behavior with very little plasticity.

Fig. 18 shows a schematic of load vs center-crack-opening displacement for a TWC pipe. For LBB applications, it is generally desired that an analysis method would underpredict the maximum load slightly. It is also desirable to underpredict the COD in the elastic range. This is because, for a given leak rate, if the COD is underpredicted then the crack length for the crack stability analysis is overpredicted. Therefore, the final maximum load in the crack stability analysis will underpredict the actual maximum load. It should also be noted that in the comparisons of crack-opening displacements, the estimation methods predict the crack-opening at the mid-thickness, whereas the experimental data (except the IPIRG-2 Experiment 1-8) have crack-opening measurements slightly above the outside diameter of the pipe. No correction was made for this difference since that would involve considerable additional effort, but this type of correction would reduce the experimental COD values slightly.

Table 6
Fracture toughness properties of pipe materials for through-wall-cracked welded pipe experiments subjected to pure bending

Pipe test no.	Extrapolated weld J–R curve parameters*		
	J_{Ic} (kJ/m^2)	C (kJ/m^2)	m
1.1.1.23	60	147.9	0.769
1.1.1.24	59	124.1	0.72
4141-1	99	164.1	0.703
4141-5	170	165.8	0.778
4111-5†	109	147.9	0.769

*J_D–R curve is represented by: $J = J_{Ic} + C(\Delta a/r)^m$ where $r = 1$ mm and Δa is in millimeters.
†Only J_{Ic} was measured and available from the material characterization test. C and m are assumed to be the same as for Experiment 1.1.1.23.

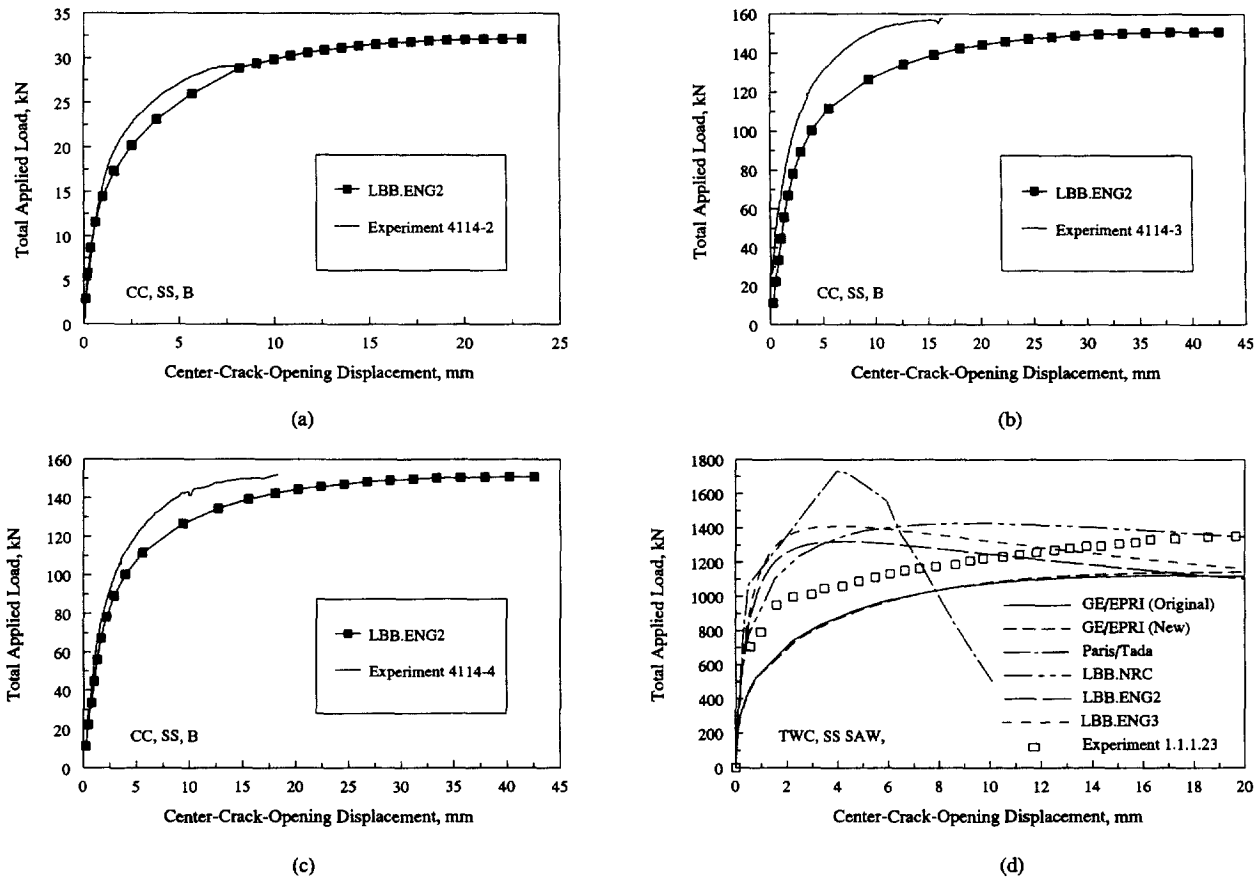

Fig. 12. Load vs center-crack-opening displacement in: (a) Experiment 4114-2; (b) Experiment 4114-3; (c) Experiment 4114-4; and (d) Experiment 1.1.1.23.

4.2. Statistics of the E/P crack-opening ratio

Standard statistical analyses were performed to assess the accuracy of the predictive models in estimating the center-crack-opening displacement for pipes analyzed in this study. The statistics involved calculation of the mean and coefficient of variation (COV) [COV is equal to the ratio of standard deviation to the mean] of the ratio between the experimental and predicted values of the center-crack-opening displacement when the applied load is 40% of the experimental maximum load. This ratio is denoted as the *E/P* crack-opening ratio for further discussion in this paper. It is desired to have this ratio greater than one to ensure smaller values of predicted crack-opening displacement than the experimental results. It should also be noted that a margin of 10 on leak-rate is generally applied in LBB analyses to account for various uncertainties including inaccuracy in crack-opening predictions [26].

4.2.1. Simple through-wall-cracked pipes

Table 8 shows the mean and COV of the *E/P* crack-opening ratio for 15 TWC pipes subjected to various loading conditions. From the results of this table, when all TWC pipe experiments are considered, all of the predictive models underpredicted the mean value of the COD. The GE/EPRI methods (with the original and newly-developed influence functions from this study) predicted experimental COD values with very good accuracy in terms of the mean value of the *E/P* crack-opening ratio, but the COVs of the *E/P* ratio showed large scatter. The differences between the statistics for the GE/EPRI method based on the original influence functions and the present study were not significant. The LBB.ENG2 and LBB.ENG3 methods slightly underpredicted the mean experimental COD with much lower COVs than those predicted by the GE/EPRI method. The LBB.NRC method underpredicted the COD more than the LBB.ENG2 or LBB.ENG3 methods with higher values of COV. Among all methods, the Paris/Tada method underpredicted the experimental COD values by the largest margin in terms of both mean and COV of the *E/P* crack-opening ratio.

Table 8 provides a further breakdown of statistics for three different loading conditions involving pure bending, pure tension and combined bending and tension. For pipes under pure bending loads, the LBB.ENG2 and LBB.ENG3 methods slightly underpredicted the experimental COD values when the mean values were compared. The LBB.NRC and Paris/Tada methods also underpredicted the COD values with the Paris/Tada method underpredicting the most. It is interesting to note that the GE/EPRI methods overpredicted the mean COD for this loading

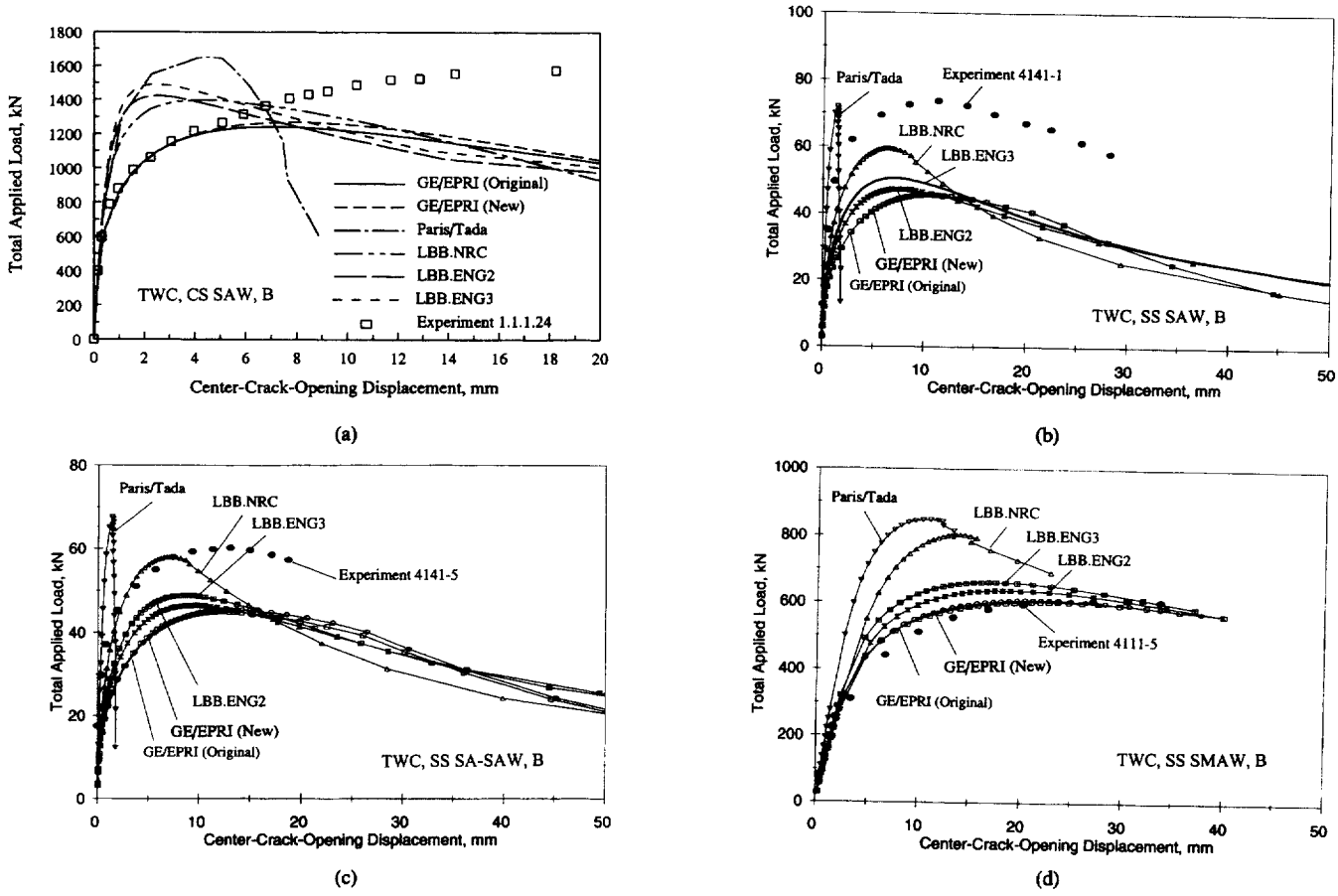

Fig. 13. Load vs center-crack-opening displacement in: (a) Experiment 1.1.1.24; (b) Experiment 4141-1; (c) Experiment 4141-5; and (d) Experiment 4111-5.

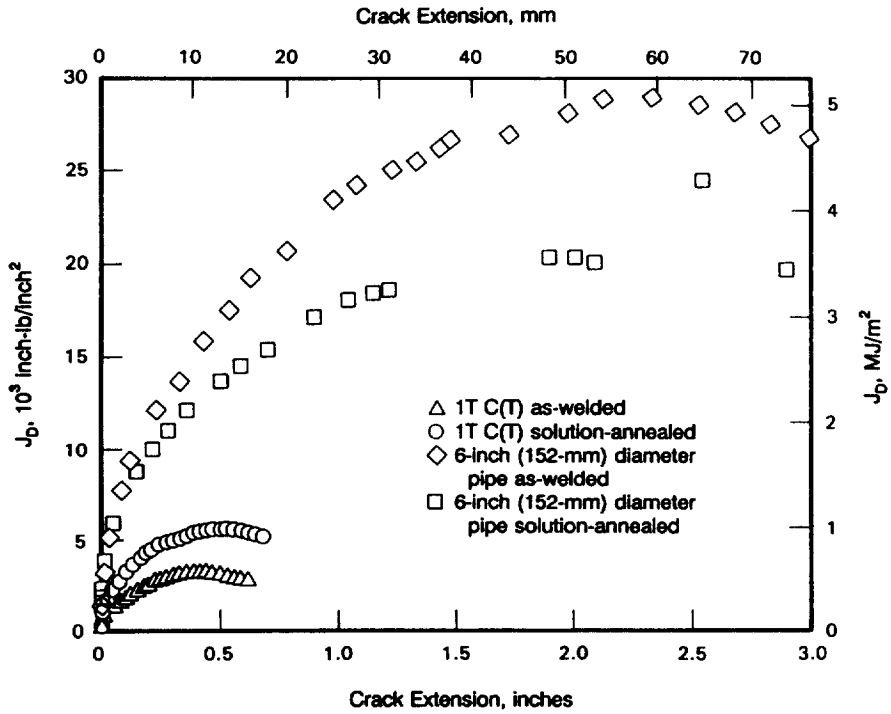

Fig. 14. Comparisons between J–R curves from 1T $C(T)$ specimens and 152.4-mm (6-in.) nominal diameter pipes via η-factor analysis.

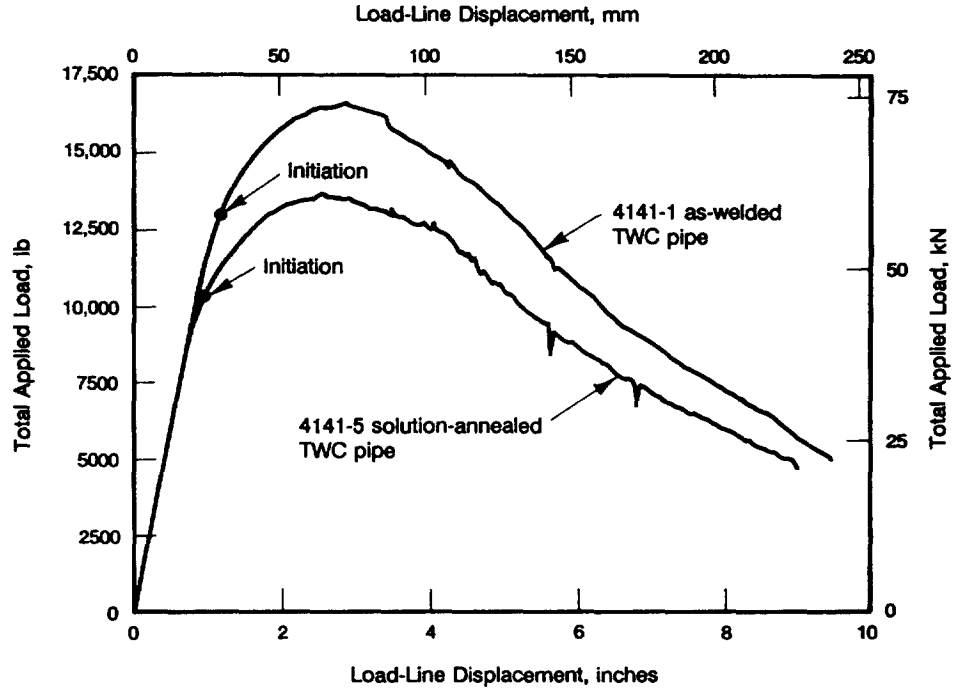

Fig. 15. Total load vs load-line displacement record from Experiments 4141-1 and 4141-5 on the 152-mm (6-in.) nominal diameter TP304 stainless steel TWC as-welded and solution-annealed SAW pipes.

condition. For a pipe under pure tension from pressure loading, similar trends were exhibited by the GE/EPRI, LBB.ENG2 and LBB.ENG3 methods. The comparisons of the COD predictions by the LBB.ENG2 and LBB.ENG3 methods with the experimental data were excellent.

For pipes under combined bending and tension, all methods considered in this study underpredicted the experimental COD. The qualitative behavior is similar to that exhibited for the results of all pipe experiments discussed earlier. On a quantitative scale, however, the magnitudes of underprediction were much higher regardless of the methods used. Once again, the Paris/Tada method significantly underpredicted the COD.

Table 9 shows the statistics of the *E/P* crack-opening ratio for pipes with short cracks ($\theta/\pi \leq 12\%$) and pipes with cracks in the girth welds. The mean results indicate that for pipes with short cracks, the crack-opening would be underpredicted by the Paris/Tada, LBB.NRC, LBB.ENG2 and LBB.ENG3 methods and overpredicted by the GE/EPRI method. A similar trend was found for pipes under pure bending. The results for pipes with cracks in girth welds also reveal a similar qualitative behavior. For the girth weld cracks, the LBB.ENG2 and LBB.ENG3 methods predicted crack-opening displacement with reasonable accuracy with mean ratios close to one.

4.2.2. Complex-cracked pipes

Table 10 shows the mean and COV of the *E/P* crack-opening ratio of 10 complex-cracked pipes under pure bending. These statistics were developed only for the

Table 7
Tensile strength and fracture toughness properties of pipe materials in a bimetallic pipe weld experiment subjected to pure bending

Pipe material	Elastic modulus (E) (GPa)	Yield stress (σ_y) (MPa)	Ultimate stress (σ_u) (MPa)	Ramberg–Osgood coefficients*		Extrapolated J–R curve parameters†		
				α	n	J_{Ic} (kJ/m^2)	C (kJ/m^2)	m
A516 Gr. 70	200	235	496	2.07	5.20	185	—‡	—‡
F316	178	157	415	9.89	3.67	2233	—‡	—‡
Inconel 182	178	372	599	3.11	8.47	ND§	ND§	ND§
A516 Gr.70/ Inconel 182	ND§	ND§	ND§	ND§	ND§	684	979.7	0.232

*Stress–strain curve is represented by: $\epsilon/\epsilon_0 = \sigma/\sigma_0 + \alpha(\sigma/\sigma_0)^n$ where $\sigma_0 = \sigma_y$, $\epsilon_0 = \sigma_0/E$.
†J_D–R curve is represented by: $J = J_{Ic}$ when $\Delta a = 0$; $J = C$ $(\Delta a/r)^m$, when $\Delta a > 0$, where $r = 1$ mm and Δa is in millimeters.
‡The power-law fit was not made for these materials.
§Not determined.

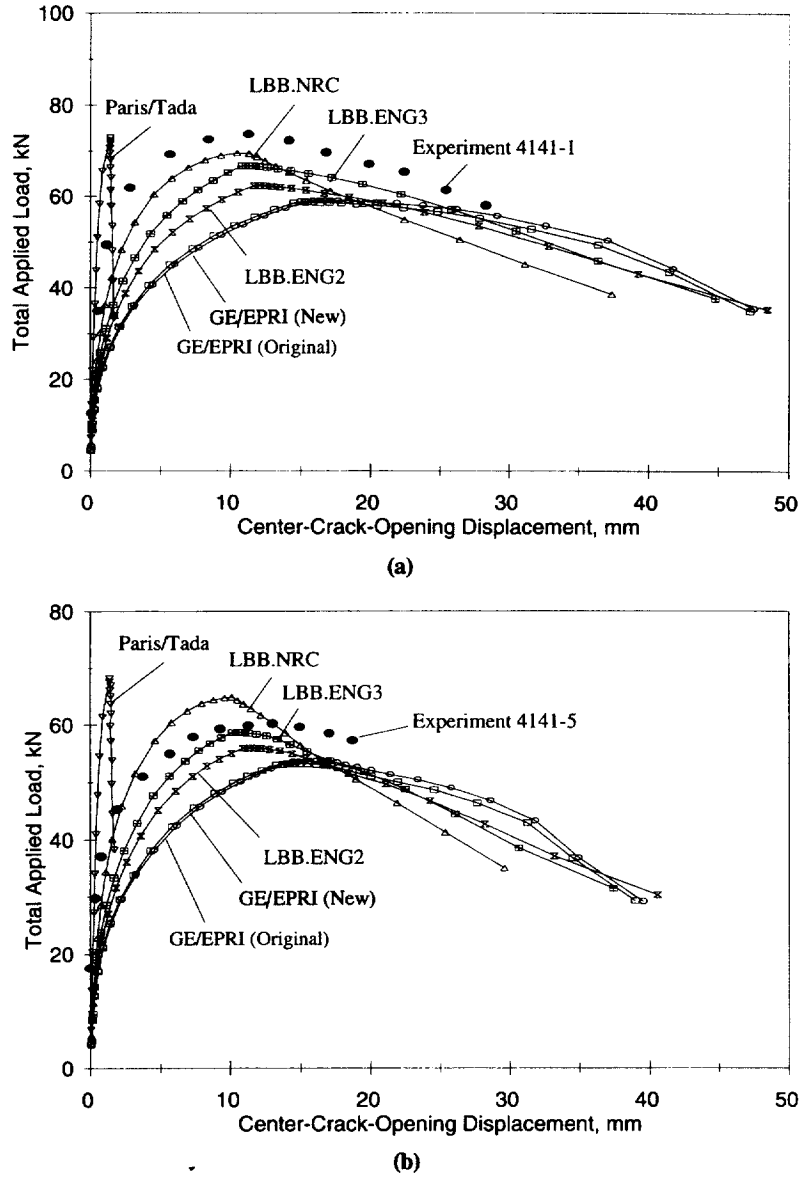

Fig. 16. Load vs center-crack-opening displacement using pipe J_D–R curves: (a) Experiment 4141-1; (b) Experiment 4141-5.

LBB.ENG2 method. The results in Table 10 suggest that the LBB.ENG2 method would overpredict (in terms of the mean value) experimental crack-opening displacement for pipes with complex cracks. This is clearly opposite to the behavior exhibited by this method in analyzing simple TWC pipes. Further breakdown of the statistics for shallow cracks ($d/t \leqslant 0.5$) and deep cracks ($d/t \geqslant 0.5$), as shown in Table 10, reveals that the estimation method provides better predictions of the experimental COD if the depth of the 360° surface crack is smaller. Nevertheless, the LBB.ENG2 predictions for complex-cracked pipes were much larger than the experimental values of the COD. As mentioned before, this overprediction of the LBB.ENG2 method is due to the oversimplification in the estimation formulas for TWC pipes used for predicting COD of complex-cracked pipes. Hence, further developments are necessary to improve the crack-opening models for complex-cracked pipes.

In analyzing pipes with a leaking crack that may potentially be a complex crack, it may not be always possible to estimate accurately the depth of the internal surface crack unless detailed nondestructive examination is performed. For such a crack, if the depth of the surface crack is overestimated, the current analysis methods would overpredict crack-opening. Hence, for a given leak rate, this will cause the crack length to be underestimated resulting in overprediction of the pipe's maximum load-carrying capacity. On the other hand, if the depth of the surface crack is underestimated or ignored, the predictive methods would underestimate crack-opening, and hence, also underestimate the load-carrying capacity of the pipe.

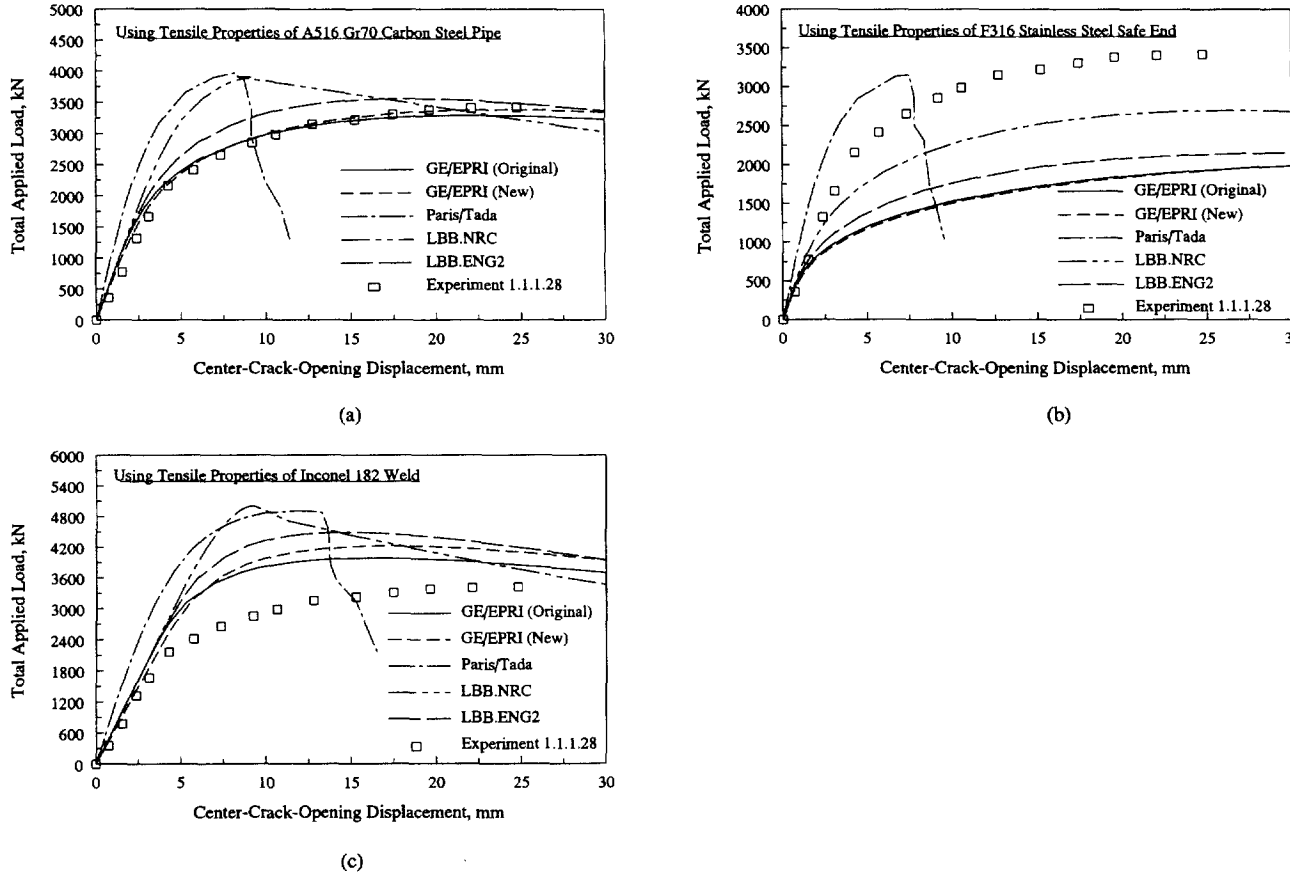

Fig. 17. Load vs center-crack-opening displacement in Experiment 1.1.1.28 using tensile properties of: (a) A516 Grade 70 carbon steel pipe; (b) F316 stainless steel safe end; and (c) Inconel 182 weld.

5. Finite element evaluations of crack-opening shapes

During this study, several finite-element analyses were performed to evaluate the adequacy of the elliptical representation of a crack-opening profile typically assumed in COA analysis. Two pipes, one with a large diameter containing a short crack and the other with a small diameter containing a long crack, were analyzed. The crack sizes are typical of leakage size flaws in LBB applications for nuclear piping systems. For the large-diameter pipe, there was one elastic analysis under pure bending. For the small-diameter pipe, there were two elastic–plastic analyses, one for pure bending and the other for combined bending and tension.

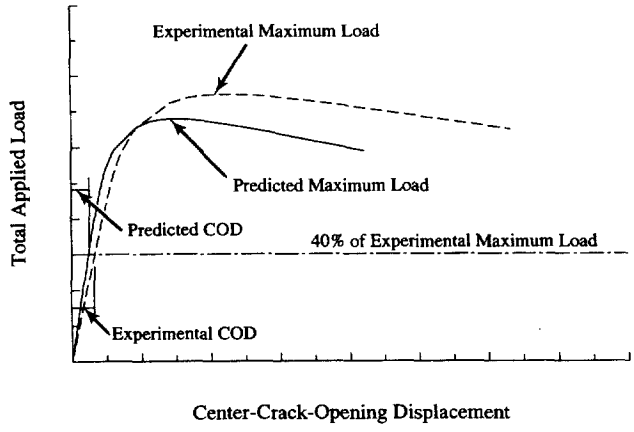

Fig. 18. Schematic comparison of predicted and experimental load vs center-crack-opening displacement in a pipe (ideally COD and load are underpredicted for LBB analyses).

5.1. Large-diameter pipes with short cracks

In this analysis, the pipe had outer diameter, D_o = 406.4 mm (16 in.), wall thickness, t = 26.19 mm (1.031 in.), crack size, θ/π = 12% and a single applied bending moment, M = 522.61 kN m (4626 inch kip). The elastic modulus, E, was 193.06 GPa (28 000 ksi) and Poisson's ratio, ν, was 0.3. The analysis was assumed to be linear–elastic with no plasticity or crack growth. Hence, the results of this analysis can be scaled for any other moments, if needed. The finite element analysis was performed by the ABAQUS code [21] with 20-noded three-dimensional solid elements. The total number of elements and nodal points were 1260 and 9030, respectively. Only one element through the thickness was used.

Fig. 19 shows the results of finite element analysis in terms of COD plotted as a function of normalized crack-tip angle, $\xi/2\theta$, where ξ is an angle from a crack tip. In this

Table 8
Mean and coefficient of variation of the ratio between experimental and predicted values of center-crack-opening displacement by various methods for simple through-wall-cracked pipes under various loading conditions

Fracture analysis methods	*E/P* ratio of center-crack-opening displacement*							
	All TWC pipes (15 tests)		TWC pipes under pure bending (11 tests)		TWC pipes under pure tension (1 test)		TWC pipes under bending and tension (3 tests)	
	Mean	Coefficient of variation† (%)	Mean	Coefficient of variation† (%)	Mean	Coefficient of variation† (%)	Mean	Coefficient of variation† (%)
GE/EPRI (original)	1.01	72.8	0.84	51.7	0.75	—‡	1.70	69.9
GE/EPRI (new)	1.02	86.5	0.74	59.5	—§	—‡	1.78	69.8
Paris/Tada	2.96	146	1.60	39.2	—§	—‡	6.59	107
LBB.NRC	1.61	90.9	1.16	47.6	—§	—‡	2.82	79.4
LBB.ENG2	1.16	47.0	1.07	45.5	1.0	—‡	1.57	41.4
LBB.ENG3	1.18	45.7	1.10	44.1	1.0	—‡	1.57	41.4

**E/P* ratio of center-crack-opening displacement = experimental center COD/predicted center COD; the CODs were measured and calculated at 40% of experimental maximum load.
†Coefficient of variation = (standard deviation/mean) × 100.
‡Not applicable.
§Not determined.

figure, two plots are shown, one for the crack-opening profile at the outer surface and the other for the crack-opening profile at the inner surface of the pipe. For each case, the continuous line indicates the crack-opening shape assuming an elliptical representation with the center COD estimated by FEM analysis. The points indicate explicit calculations by FEM as a function of $\xi/2\theta$. It appears that both outer and inner crack-opening profiles can be accurately modeled by an elliptical shape.

5.2. Small-diameter pipes with long cracks

To understand the crack-opening characteristics for long cracks in small-diameter pipes, additional finite element computations were also made in this study. In this case, the pipe had mean diameter, $D_m = 101.6$ (4 in.), wall thickness, $t = 8.56$ mm (0.337 in.) and crack size, $\theta/\pi = 37\%$. Two loading cases were studied: (1) pure bending; and (2) combined bending and tension (pressure induced) with 15.51 MPa (2250 psi) internal pressure. For each loading case, the results due to several values of moment were investigated. The internal pressure in the pipe was simulated by applying the axial (tension) force only. Neither hoop stress nor crack-face pressure were modeled.

The elastic modulus and Poisson's ratio were 193.06 GPa (28 000 ksi) and 0.29, respectively. The analyses were elastic–plastic and, therefore, a nonlinear stress–strain curve for the pipe material needs to be specified as well. In this regard, the Ramberg–Osgood model, defined in Rahman et al. [1] [see Eq. (1) of this reference], was chosen to represent the tensile properties with the following parameters: $\sigma_0 = 210$ MPa (30.5 ksi), $\alpha = 2.6$ and $n = 4.06$. The crack length was held constant for all applied loads.

The finite element analyses were performed by the ABAQUS code [21] with 20-noded three-dimensional solid elements. The total number of elements and nodal points were 949 and 4984, respectively. There were four elements through the thickness. The size (length along the

Table 9
Mean and coefficient of variation of the ratio between experimental and predicted values of center-crack-open displacement by various methods for simple through-wall-cracked pipes with short cracks and cracks in girth welds

Fracture analysis methods	*E/P* ratio of center-crack-opening displacement*			
	TWC pipes with short cracks ($\theta/\pi \leq 0.12$) (4 tests)		TWC pipes with cracks in girth welds (6 tests)	
	Mean	Coefficient of variation† (%)	Mean	Coefficient of variation† (%)
GE/EPRI (original)	0.74	31.0	0.67	70.4
GE/EPRI (new)	0.76	36.0	0.62	67.0
Paris/Tada	1.42	37.2	1.61	33.5
LBB.NRC	1.30	21.4	1.04	45.1
LBB.ENG2	1.45	26.8	1.01	58.3
LBB.ENG3	1.47	27.3	1.06	55.3

**E/P* ratio of center-crack-opening displacement = experimental center COD/predicted center COD; the CODs were measured and calculated at 40% of experimental maximum load.
†Coefficient of variation = (standard deviation/mean) × 100.

Table 10
Mean and coefficient of variation of the ratio between experimental and predicted values of center-crack-opening displacement by the LBB.ENG2 method for complex-cracked pipes with shallow and deep surface cracks

Fracture analysis methods	*E/P* ratio of center-crack-opening displacement*					
	All CC pipes (10 tests)		CC pipes with shallow cracks ($d/t \leq 0.5$) (7 tests)		CC pipes with deep cracks ($d/t \geq 0.5$) (3 tests)	
	Mean	Coefficient of variation† (%)	Mean	Coefficient of variation† (%)	Mean	Coefficient of variation† (%)
LBB.ENG2	0.63	41.5	0.77	24.7	0.33	36.5

**E/P* ratio of center-crack-opening displacement = experimental center COD/predicted center COD; the CODs were measured and calculated at 40% of experimental maximum load.
†Coefficient of variation = (standard deviation/mean) × 100.

cracked plane) of the smallest element near the crack tip was 0.051 mm (0.002 in.).

The crack-opening displacements calculated by the FEM at the mid-thickness level of the pipe are given in Figs 20 and 21. Fig. 20 shows several plots of crack-opening displacement as a function of the normalized crack angle from the crack tip ($\xi/2\theta$) for several bending moments without any internal pressure. Similar results are plotted in Fig. 21 for the pipe under combined bending and tension with four different moments. The crack-opening shapes based on elliptical representations with crack length as the major axis and the center COD as the minor axis are also shown. The comparisons between finite element results (points) and the elliptical equation (lines) suggest that for a stationary crack the crack-opening profile can indeed be closely modeled by an elliptical shape, regardless of load intensity and hence, the amount of plasticity in the cracked pipe.

For very large moments, the crack-driving force (applied J) was much higher than typical fracture initiation toughness (J_{Ic}) of austenitic or ferritic materials. This explains why there were slight crack-tip blunting in the finite element calculations in which no crack growth was allowed.

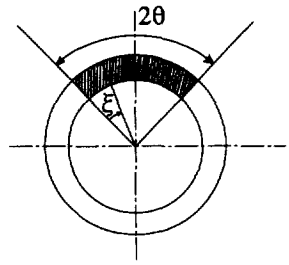

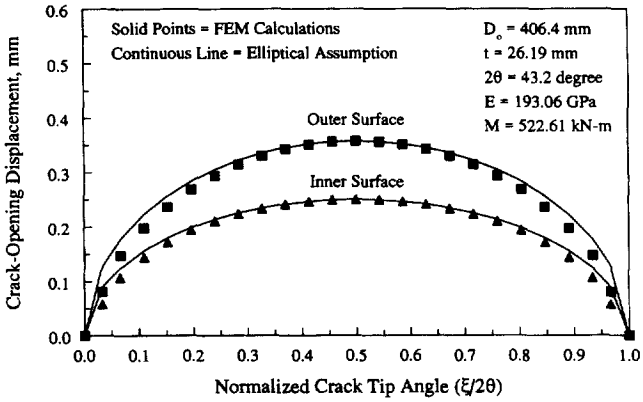

Fig. 19. Crack-opening shape for a large-diameter pipe with a short cack under pure bending (elastic analysis).

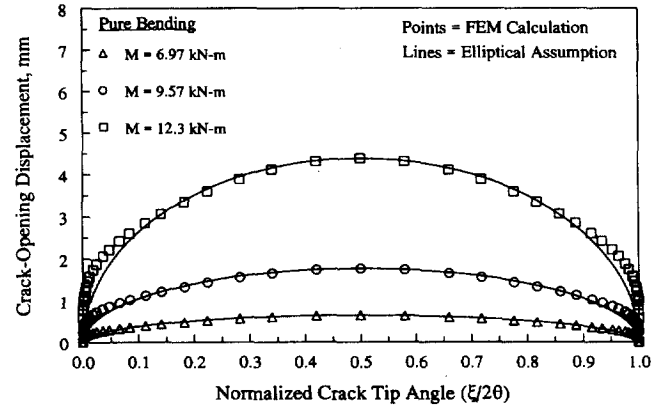

Fig. 20. Crack-opening shape for a small-diameter pipe with a long crack under pure bending (elastic–plastic analysis).

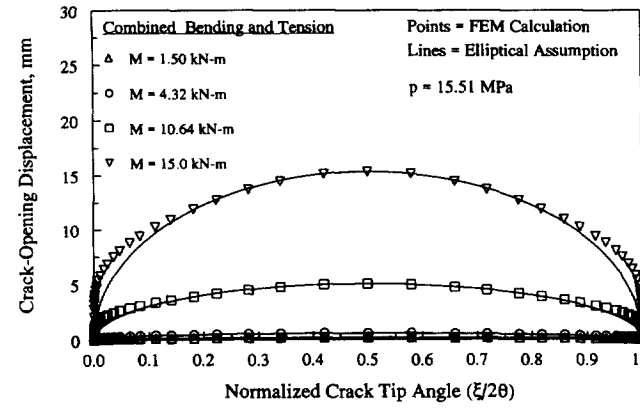

Fig. 21. Crack-opening shape for a small-diameter pipe with a long crack under combined bending and tension (elastic–plastic analysis).

6. Conclusions

Twenty-five pipe experiments were analyzed to detertmine the accuracy of clurrent estimation models for predicting center-crack-opening displacement for pipes with simple through-wall and complex cracks. Standard statistical analyses were performed to determine the statistics (mean and COV) of the *E/P* crack-opening ratio when the applied load was 40% of the experimental maximum load. (Note, the fracture behavior at this load is primarily elastic.) The results showed the following.

6.1. From analyses of simple through-wall-cracked pipes

(1) When all TWC pipe experiments were considered, all of the predictive models underpredicted the mean value of the experimental COD values (i.e. mean ratio greater than 1). The GE/EPRI methods (with the original and newly developed influence functions from this work) predicted experimental COD values with very good accuracy in terms of the mean value of the *E/P* crack-opening ratio, but their predicted COVs showed large scatter. The differences between the statistics for the GE/EPRI method based on the original influence functions and those from the present study were not significant. The LBB.ENG2 and LBB.ENG3 methods slightly underpredicted the mean experimental COD values with much lower COVs than those predicted by the GE/EPRI method. The LBB.NRC method underpredicted the experimental COD values more than the LBB.ENG2 or LBB.ENG3 methods with higher values of COV. Among all methods, the Paris/Tada method underpredicted the experimental COD values by the largest margin in terms of both mean and COV of the *E/P* crack-opening ratio.

(2) The mean results for pipes with short cracks (3 pipes under pure bending and 1 pipe under combined bending and tension) indicate that the experimental crack-opening would be underpredicted by the Paris/Tada, LBB.NRC, LBB.ENG2 and LBB.ENG3 methods and overpredicted by the GE/EPRI method. A similar trend was found for all pipes under pure bending. The results for pipes with cracks in girth welds also reveal a similar qualitative behavior. For the girth weld cracks, the LBB.ENG2 and LBB.ENG3 methods predicted experimental crack-opening displacement with reasonable accuracy with mean ratios close to one.

(3) It is worth noting that the COV of the *E/P* crack-opening ratio for all TWC pipes considered in this study varied from 46 to 146%. From a separate study by the authors [24], the COV of the *E/P* maximum load ratio for TWC pipes was only 10–26%. Hence, further study is needed for improving the crack-opening-area models.

6.2. From analyses of complex-cracked pipes

(1) Complex-cracked pipe experiments, i.e. a pipe with a 360° circumferential surface crack and a finite length through-wall crack, were also analyzed using only the LBB.ENG2 method. The LBB.ENG2 method overpredicted (in terms of the mean value) crack-opening displacement for pipes with complex cracks. This is clearly opposite to the behavior exhibited by this method in analyzing simple through-wall-cracked pipes. Further breakdown of the statistics for shallow cracks ($d/t \leqslant 0.5$) and deep cracks ($d/t \geqslant 0.5$) reveals that this estimation method provides better predictions of the experimental COD if the depth of the 360° surface crack is smaller. For example, the mean values of the crack-opening ratio were 0.77 for shallow cracks and 0.33 for deep cracks. Nevertheless, the LBB.ENG2 predictions for complex-cracked pipes were much larger than the experimental COD values. This overprediction of the LBB.ENG2 method is due to the oversimplification in the estimation formulas for TWC pipes used for predicting the COD of complex-cracked pipes. Hence, further developments are necessary to improve crack-opening models for complex-cracked pipes.

6.3. From finite element analyses

(1) The finite element predictions of the center-crack-opening displacement for Experiment 1.1.1.21 containing a short through-wall crack ($\theta/\pi = 6.25\%$) were in very good agreement with the experimental data from the pipe test.

(2) The results from several finite element analyses showed that the crack-opening shape for a pipe would approximately follow an elliptical profile. Both large-diameter pipes with short cracks and small-diameter pipes with long cracks were analyzed under pure bending and combined bending plus tension to reach this conclusion.

Acknowledgements

The authors would like to thank Mr Michael Mayfield and the US NRC Office of Research, Electrical, Materials and Mechanical Engineering Branch for their encouragement and support of this effort as part of the US NRC's 'Short Cracks in Piping and Piping Welds' program, contract no. NRC-04-90-069. Their support and guidance are sincerely appreciated. The authors would also like to thank Dr R. Mohan of Battelle for performing a few finite element analyses and Dr N. Miura of CRIEPI for developing some plots.

References

[1] Rahman S, Brust FW, Ghadiali N, Wilkowski G. Crack-opening area analyses for circumferential through-wall cracks in pipes—Part I: Analytical Models. International Journal of Pressure Vessels and Piping, 1998;75:357–373.

[2] Kumar V, German M, Shih C. An engineering approach for elastic–plastic-fracture analysis. EPRI Report NP-1931. Palo Alto, CA: Electric Power Research Institute, 1981.

[3] Kumar V, German M, Wilkening W, Andrews W, deLorenzi H, Mowbray D. Advances in elastic–plastic fracture analysis. EPRI Final Report NP-3607. Palo Alto, CA: Electric Power Research Institute, 1984.

[4] Kishida K, Zahoor A. Crack-opening area calculations for circumferential through-wall-pipe cracks. EPRI Special Report NP-5959-SR. Palo Alto, CA: Electric Power Research Institute, 1988.

[5] Paris PC, Tada H. The application of fracture proof design methods using tearing stability theory to nuclear-piping postulating-circumferential through-wall cracks. NUREG/CR-3464. Washington, DC: US Nuclear Regulatory Commission, 1983.

[6] Klecker R, Brust F, Wilkowski G. NRC leak-before-break (LBB.NRC) analysis method for circumferentially through-wall-cracked pipes under axial plus bending loads. NUREG/CR-4572. Washington, DC: US Nuclear Regulatory Commission, 1986.

[7] Brust FW. Approximate-methods for fracture-analyses of through-wall cracked pipes. NUREG/CR-4853. Washington, DC: US Nuclear Regulatory Conunission, 1987.

[8] Gilles P, Brust F. Approximate fracture methods for pipes. Part I—Theory. Nuclear Engineering and Design, 1991;127:1–27.

[9] Gilles P, Chao KS, Brust F. Approximate fracture methods for pipes. Part II—Applications. Nuclear Engineering and Design, 1991;127: 13–31.

[10] Rahman S, Brust F, Nakagaki M, Gilles P. An approximate method for estimating energy release rates of through-wall cracked pipe weldments. Fatigue, Fracture and Risk 1991; (215) ASME, San Diego, CA.

[11] Rahman S, Brust F. An estimation method for evaluating energy release-rates of circumferential through-wall cracked pipe welds. Engineering Fracture Mechanics, 1992;43(3):417–430.

[12] Rahman S, Brust F. Elastic–plastic fracture of circumferential through-wall cracked pipe-welds subject to bending. Journal of Pressure Vessel Technology, 1992;114(4):410–416.

[13] Wilkowski GM, Ahmad J, Barnes CR, Brust F, Ghadiali N, Guerrieri D, Jones D, Kramer G, Landow M, Marschall CW, Olson R, Papaspyroppulos V, Pasupathi V, Rosenfeld M, Scott P, Vieth P. Degraded piping program—Phase II. Summary of technical results and their significance to leak-before-break and in-service flaw acceptance criteria. NUREG/CR-4082, Vol. 8. Washington, DC: US Nuclear Regulatory Commission, 1989.

[14] Schmidt RA, Wilkowski GM, Mayfield ME. The international piping integrity research group (IPIRG) program: an overview. In: H. Shibata, editor, Transactions of the 11th International Conference on Structural Mechanics in Reactor Technology, Vol. G2: Fracture Mechanics and Non-Destructive Evaluation-2. Tokyo, Japan, paper no. G23/1, 1991:177–188.

[15] Hopper A, Mayfield M, Olson R, Scott P, Wilkowski G. Overview of the IPIRG-2 Program—seismic loaded cracked pipe system experiments. In: 13th International Conference on Structural Mechanics in Reactor Technology, Division F, Paper F12-1, 1995.

[16] Wilkowski G. et al. Short cracks in piping and piping program. Semi-annual reports by Battelle. NUREG/CR-4599, Vol. 1–3, nos. 1–2. Washington, DC: US Nuclear Regulatory Commission, 1991–1994.

[17] Rahman S, Ghadiali N, Wilkowski G, Moberg F, Brickstad B. Crack-opening analyses for circumferential through-wall cracks in pipes—Part III: Off-center cracks, restraint of bending, thickness transition and weld residual stresses. International Journal of Pressure Vessels and Piping, 1998;75:397–415.

[18] Paul D, Ahmad J, Scott P, Flanigan L, Wilkowski G. Evaluation and refinement of leak-rate estimation models. NUREG/CR-5128, Rev. 1. Washington, DC: US Nuclear Regulatory Commission, 1994.

[19] Kanninen MF et al., Instability predictions for circumferentially tracked Type-304 stainless steel pipes under dynamic loading—Vol. 2. Appendices. EPRI Report NP-2347, Vol. 2. Palo Alto, CA: Electric Power Research Institute, April 1982.

[20] Rahman S, Brust F, Ghadiali N, Choi YH, Krishnaswamy P, Moberg F, Brickstad B, Wilkowski G. Refinement and evaluation of crack-opening area-analyses for circumferential through-wall cracks in pipes. NUREG/CR-6300. Washington, DC: US Nuclear Regulatory Commission, 1995.

[21] ABAQUS, user's guide and theoretical manual, Version 5.3. Pawtucket, RI: Hibbitt, Karlsson & Sorensen, 1993.

[22] Wilkowski G, Ahmad J, Brust F, Guerrieri D, Kramer G, Kulhowvick G, Landow M, Marschall C, Nakagaki M, Papaspyropoulos V, Scott P. Analysis of experiments on stainless steel flux weld. NUREG/CR-4878. Washington, DC: US Nuclear Regulatory Commission, 1987.

[23] Rahman S, Wilkowski G, Brust F. Analysis of full-scale pipe fracture experiments on stainless steel flux welds. In: G. Wilkowski, editor, Fatigue, flaw evaluation, and leak-before-break assessments—1994, ASME Special Publication, ASME, 1994:280.

[24] Brust FW, Scott P, Rahman S, Ghadiali N, Kilinski T, Francini B, Marschall C, Miura N, Krishnaswamy P, Wilkowski G. Assessment of short through-wall circumferential cracks in pipes. NUREG/CR-6235. Washington, DC: US Nuclear Regulatory Commission, 1995.

[25] ASTM Standard E1152-87, Standard test method for determining J–R curve. In: Annual Book of ASTM Standards, Vol. 03.01., ASTM, 1991.

[26] Report to the US Nuclear Regulatory Commission Piping Review Committee Prepared by the Pipe Break Task Group, NUREG/CR-1061, Vol. 3. Washington, DC: US Nuclear Regulatory Commission, 1984.